AN ASYMPTOTIC SOLUTION FOR THE FLOW ABOUT AN ELLIPSOID NEAR A PLANE WALL

Thesis by

Phillip Eisenberg

In Partial Fulfillment of the Requirements for the Degree of Civil Engineer

California Institute of Technology
Pasadena, California

May, 1948

ACKNOWLEDGEMENT

The author is most appreciative of the interest and encouragement of his supervising committee -- Professors R. R. Martel, R. T. Knapp, and H. J. Stewart -- and of Dr. M. S. Plesset, who suggested the problem.

He is especially indebted to Dr. H. J. Stewart for his suggestions and for giving so unstintingly of his time for the discussion of this and related problems of interest to the author.

To Dr. R. T. Knapp, Director of the Hydrodynamics Laboratory, where the program was conducted, the writer is deeply grateful for facilitating the work in every possible way and for making available the assistance of laboratory personnel despite an already crowded program. Among the latter, special thanks are due Messrs. J. P. O'Neil, D. Baron, A. M. Taylor, and M. Bidwell, for their assistance in the experiments and the preparation of equipment and models, Mr. J. H. Beveridge for many numerical computations, Miss Wesley Metcalf for the preparation of tracings, and Miss Althea Pease and Mr. J. Savage for the photographs.

ABSTRACT

The inherent difficulties in obtaining the solution for the flow about arbitrary bodies of revolution near a wall usually precludes an exact evaluation of the effect of wall proximity on the pressure distributions. However, many bodies of revolution may be replaced with good approximation by an ovary ellipsoid. For this purpose, an approximate solution for the velocity potential is obtained for the flow about an ellipsoid near a plane wall which approaches the exact solution in an infinite stream as the ellipsoid recedes from the wall.

The evaluation of the image potentials and rectifying images is accomplished by an expansion in associated Legendre polynomials. A first approximation, which results in a symmetric distribution on the ellipsoid, is essentially an expansion in associated Legendre polynomials of zero order. A second approximation, which correctly predicts differences of pressure on opposite sides of the ellipsoid, is carried out by an exact evaluation of the effects of the image potentials while evaluating the rectifying images by the same method as followed for the first approximation. The solutions are obtained in closed form with resulting expressions for the velocity and pressure distributions that are especially convenient for application to specific cases.

The solutions are compared with pressure distributions measured on two ellipsoid models placed near a plate, simu-

lating a wall, in the free surface flume of the Hydrodynamics Laboratory. The first approximation shows good agreement along the meridian parallel to the wall but rather large deviations at other points of the ellipsoids. This approximation is probably most useful only for estimates of the change in pressure distribution for varying separations, and where a high degree of precision in actual values is not required.

The second approximation, on the other hand, shows very good agreement for distances even as small as one diameter from the center of the ellipsoid to the wall. For smaller distances this approximation shows large deviations at the minimum pressure point of the half-meridian closest to the wall with increasing accuracy for points on the ellipsoid that are farther from the wall.

TABLE OF CONTENTS

LIST OF FIGURES

AN ASYMPTOTIC SOLUTION FOR THE FLOW ABOUT AN ELLIPSOID NEAR A PLANE WALL

Introduction

The variable-pressure water tunnel (1)(2)(3)(4)* has for some years been an important facility in hydrodynamical research for application to the design and performance of ships' propellers and water turbine impellers under cavitating as well as non-cavitating conditions. For more fundamental investigations of the mechanics of the cavitation phenomenon, it has been found fruitful to study the behavior of cavitating flows resulting from the flow about bodies of revolution (5)(6). In this connection, as well as for more general studies in the water tunnel or open flume of the flow about bodies of revolution, the influence of proximate tunnel walls on the pressure distributions is of importance. These effects also form one of the major considerations in the selection of proportions in the design of towing basins for tests of both surface and submerged models. Other engineering applications in which the influence of "walls" on water flows are of interest include the movement of vessels in shallow channels and narrow canals.

The effects of wall interference on the flow about lifting systems have been investigated in rather thorough

---

* Numbers in parentheses indicate references on page 35.

detail in connection with wind tunnel research (see e.g. (7)(8)), and somewhat less extensively for non-lifting systems (7)(9)(10). The corrections available from these solutions, however, must be obtained by rather laborious summations in series with resultant loss of appeal for more or less rapid checks on interference effects and for preliminary design purposes. As a result, it would be of convenience to have the solution for a body of revolution which can be used easily as an approximation to the actual form considered, and for which the resulting expressions are not too unwieldy.

For this purpose, it is proposed to use an ellipsoid of revolution. Many bodies of revolution may be replaced by an ellipsoid with good approximation by holding constant the lengths and displacements, provided the nose and tail curvatures of these bodies do not vary too rapidly. For the effect on the wall, the approximation may be expected to be even better, provided the body is of the order of one or two diameters from the wall. In the case of ships near a shallow bottom, the hull of the vessel might be replaced by the lower half of an ellipsoid, in which case the water surface of the canal must be treated as a plane of symmetry. In the latter case, it would probably be more accurate to hold constant the draft and the displacement.

Although the problem treated hereafter applies only to the case of an ellipsoid near a single, plane wall, it

can be used to give approximately the first order effect of each wall singly in such applications as a rectangular water tunnel or model basin and of the bounding image planes in the case of a vessel in a shallow channel.

The solution as obtained in this paper is in closed form with expressions that are quite easily applied to specific cases. The accuracy of the solution was tested by measurements of the pressure distributions on two ellipsoid models. Comparisons of the calculated and measured values for the models at various distances from a single wall are included.

OVARY ELLIPSOIDAL COORDINATES AND THE CORRESPONDING EQUATION OF CONTINUITY

It is convenient for most treatments of potential flows about completely submerged bodies to employ a coordinate system in which one of the constant coordinate lines or surfaces coincides with the particular form under study. For the present problem, the so-called ovary ellipsoidal or semi-elliptic coordinates are applicable (11)(12). The origin of coordinates is chosen to coincide with the center of the ellipsoid having foci in cartesian coordinates placed at $x = \pm c$, $y = z = 0$, (lower half of Figure 1). Planes through any meridian section of the ellipsoid make an angle ω with the x-y plane. The ellipsoidal coordinates, μ, ξ, ω, are then defined by the set of equations

$$\left.\begin{aligned} x &= c\mu\xi \\ \bar{y} &= c\sqrt{(1-\mu^2)(\xi^2-1)} \\ \omega &= \omega \end{aligned}\right\} \quad [1]$$

It is clear that $\bar{y}$ is the distance perpendicular to the x-direction in the plane ω = constant, and that the cartesian coordinate $y = \bar{y}\cos\omega$. From [1], the surfaces ξ = constant are represented by the relation

$$\frac{x^2}{c^2\xi^2} + \frac{\bar{y}}{c^2(\xi^2-1)} = 1 \quad [2]$$

and the surfaces μ = constant are given by

$$\frac{x^2}{c^2\mu^2} - \frac{\bar{y}}{c^2(1-\mu^2)} = 1 \quad [3]$$

Equation [2] represents a set of ellipsoidal surfaces confocal with the ellipsoid and having semi-major axes equal to $c\xi$ and semi-minor axes equal to $c\sqrt{\xi^2-1}$. Equation [3] represents a set of confocal hyperboloids with foci at $x = \pm c$ and semi-axes $c\mu$ and $c\sqrt{1-\mu^2}$.

Elements of arc length ds in the direction of increasing μ, ξ, and ω are readily shown to be

$$\left.\begin{aligned} ds_\mu &= c\sqrt{\frac{\xi^2-\mu^2}{1-\mu^2}}\,d\mu \\ ds_\xi &= c\sqrt{\frac{\xi^2-\mu^2}{\xi^2-1}}\,d\xi \\ ds_\omega &= c\sqrt{(1-\mu^2)(\xi^2-1)}\,d\omega \end{aligned}\right\} \quad [4]$$

From the definition of the velocity potential Φ as the integral of the scalar product of the length of line element and the velocity vector, the velocity components in the directions of increasing μ, ξ, and ω are*

$$\left.\begin{aligned} u_\mu &= -\frac{\partial \Phi}{\partial s_\mu} = -\frac{\partial \Phi}{\partial \mu}\frac{\partial \mu}{\partial s_\mu} = -\frac{1}{c}\sqrt{\frac{1-\mu^2}{\xi^2-\mu^2}}\ \frac{\partial \Phi}{\partial \mu} \\ u_\xi &= -\frac{\partial \Phi}{\partial s_\xi} = -\frac{\partial \Phi}{\partial \xi}\frac{\partial \xi}{\partial s_\xi} = -\frac{1}{c}\sqrt{\frac{\xi^2-1}{\xi^2-\mu^2}}\ \frac{\partial \Phi}{\partial \xi} \\ u_\omega &= -\frac{\partial \Phi}{\partial s_\omega} = -\frac{\partial \Phi}{\partial \omega}\frac{\partial \omega}{\partial s_\omega} = -\frac{1}{c\sqrt{(1-\mu^2)(\xi^2-1)}}\ \frac{\partial \Phi}{\partial \omega} \end{aligned}\right\} \quad [5]$$

Replacing these velocity components in the equation of continuity for an incompressible fluid

$$\nabla \cdot (u_\mu, u_\xi, u_\omega) = 0$$

by their appropriate definition [5] gives the Laplace equation of continuity in these coordinates

$$\frac{\partial}{\partial \mu}\left[(1-\mu^2)\frac{\partial \Phi}{\partial \mu}\right] + \frac{\partial}{\partial \xi}\left[(\xi^2-1)\frac{\partial \Phi}{\partial \xi}\right] + \frac{\xi^2-\mu^2}{(1-\mu^2)(\xi^2-1)}\frac{\partial^2 \Phi}{\partial \omega^2} = 0 \quad [6]$$

The potential which satisfies the boundary conditions of the problem and is a solution of [6] will give the correct flow configuration.

---

* To avoid confusion between the present results and the references cited, Lamb's (11) sign convention is used throughout in the definition of the velocity in irrotational motion as the gradient of a potential.

THE SOLUTION FOR AN OVARY ELLIPSOID IN AN INFINITE STREAM

The solution for the flow about an ovary ellipsoid moving parallel to its major axis, which forms the starting point of the present investigation, is given by Lamb (11). In general, the solutions of equation [6] for the case of symmetry are

$$\left.\begin{aligned} \Phi &= P_n(\mu)\, P_n(\xi) \\ \Phi &= P_n(\mu)\, Q_n(\xi) \end{aligned}\right\} \qquad [7]$$

where the $P_n(\mu)$ and $P_n(\xi)$ are the so-called zonal surface harmonics of the first kind or Legendre coefficients, and the $Q_n(\xi)$ are zonal harmonics of the second kind (13). The zonal harmonics which are applicable to the case in which the flow pattern is identical in every meridianal plane correspond to integral values of n in the formula (14)

$$P_n(\mu) = \frac{1}{2^n n!} \frac{d^n}{d\mu^n} (\mu^2 - 1)^n \qquad [8]$$

and the corresponding expression for $P_n(\xi)$. The $Q_n(\xi)$ are given by (11)

$$Q_n(\xi) = P_n(\xi) \int_{\xi}^{\infty} \frac{d\xi}{(\xi^2 - 1)\{P_n(\xi)\}^2} \qquad [9]$$

For a single ellipsoid moving with velocity U in a fluid otherwise at rest, the boundary condition at the surface $\xi = \xi_0 = \frac{1}{e_0}$, where e_0 is the eccentricity of the ellipsoid, is

$$\frac{\partial \Phi}{\partial s_\xi} = -U \frac{\partial x}{\partial s_\xi}$$

or, using [1],

$$\frac{\partial \Phi}{\partial \xi} = -U \frac{\partial x}{\partial \xi} = -Uc\mu \qquad [10]$$

With this condition and the conditions that the fluid be stationary at infinity, the solution as shown by Lamb is

$$\Phi = A P_1(\mu) Q_1(\xi) = A\mu \left\{ \frac{1}{2} \xi \ln \frac{\xi+1}{\xi-1} - 1 \right\} \qquad [11]$$

where

$$A = \frac{Uc}{\frac{e_o}{1-e_o^2} - \frac{1}{2} \ln \frac{1+e_o}{1-e_o}} \qquad [12]$$

In this case, the flow pattern is symmetric with respect to any axis of the ellipsoid so that a stream function also can be shown to exist. However, since no corresponding stream function exists for the ellipsoid near a wall, a discussion of this function is omitted here.

FORMULATION OF THE PROBLEM OF FLOW ABOUT AN ELLIPSOID NEAR A PLANE WALL

It is clear that the solution of the problem of flow about an ellipsoid near a plane wall is known if the solution is known for the flow about two ellipsoids of the same size moving abreast at the same speed. Here, the plane of symmetry halfway between the two forms is a stream surface and may be replaced by a solid "wall" without disturbing the motion. This type of solution requires the determina-

tion of the source distributions in the ellipsoid and its image which leave these stream surfaces undeformed. Another type of solution is based on an appropriate distribution of sources which, in a uniform stream, form the wall and the solid body, but are located only within the ellipsoid and outside the field of flow about the ellipsoid. The latter procedure reduces to finding Green's function* for the boundary conditions that the ellipsoidal surface and the wall be stream surfaces.

The solution obtained herein is based on the first method outlined above. If the solution is known for the translatory motion of a single body in an infinite stream, this solution may be used as the starting point for the case of two such bodies. The potential of the single form will then induce a potential on the other which results in a cross flow violating the condition that this surface be a stream surface. To restore the original shape of this second body, a distribution within the body of, in general, sources, sinks, and doublets must be found that produce velocity components that just cancel the effects of the original potential. This distribution constitutes the image of the original potential. However, the image potential, thus found, in turn deforms the first body which must be

---

* A number of examples of the application of Green's function to certain boundary value problems are worked out in Reference (15).

restored by a similar procedure. This process is then carried through until the effects of all the images are rectified. To complete the solution, the process is repeated starting with the infinite stream potential of the second body. Although this method of obtaining a solution is, in principle, quite clear, the exact evaluation of the strengths and positions of successive images in specific cases may be extremely laborious if not also difficult. It is shown in the subsequent discussion that this situation occurs in the case of flow about two ellipsoids. As a result, the present solution is obtained from an approximate evaluation of the image strengths and types required to cancel the induced potentials on the "real" ellipsoid due to the presence of the image ellipsoid.

The model used for the computation is shown in Figure 1, wherein the primed ellipsoidal coordinate system refers to the image. The ellipsoids, which have semi-major diameters a and semi-minor diameters b, are assumed to be separated by a distance 2h. From equation [1] and the triangle OO'P in Figure 1, it is seen that the two coordinate systems are related by

$$x = c\mu\xi = c\mu'\xi' \qquad [1']$$

and

$$\bar{y}'^2 = \bar{y}^2 + 4h^2 - 4h\bar{y}\cos\omega \qquad [13]$$

The velocity potential which is a solution of equation [6] for this problem will be of the form

$$\Phi = \varphi + \varphi' \qquad [14]$$

where φ is the potential of the real ellipsoid and φ' the potential of the image. In order that the model be undeformed, there must be no cross-flow through the surfaces of the two ellipsoids. This requirement and the boundary condition [10] impose the boundary conditions on the real ellipsoid, $\xi = \xi_o = \frac{1}{e_o}$,

$$\frac{\partial \varphi}{\partial \xi} = -Uc\mu \quad \text{and} \quad \frac{\partial \varphi'}{\partial \xi} = 0 \qquad [15]$$

and, on the image ellipsoid, $\xi' = \xi_o' = \frac{1}{e_o}$,

$$\frac{\partial \varphi}{\partial \xi'} = 0 \quad \text{and} \quad \frac{\partial \varphi'}{\partial \xi'} = -Uc\mu' \qquad [16]$$

Since this case is not one of symmetry in the sense of the single ellipsoid in an infinite stream, the solutions will no longer be of the form [7], but will be of the types

$$\left.\begin{aligned} \Phi &= P_n^m(\mu)\, P_n^m(\xi) \begin{Bmatrix} \cos \\ \sin \end{Bmatrix} m\omega \\ \text{and} \\ \Phi &= P_n^m(\mu)\, Q_n^m(\xi) \begin{Bmatrix} \cos \\ \sin \end{Bmatrix} m\omega \end{aligned}\right\} \qquad [17]$$

Where the $P_n^m(\mu)$, $P_n^m(\xi)$ and $Q_n^m(\xi)$, the so-called associated Legendre polynomials (16), are defined by

$$P_n^m(\mu) = (1-\mu^2)^{\frac{m}{2}} \frac{d^m P_n(\mu)}{d\mu^m}$$

and

$$\left.\begin{matrix} P_n^m(\xi) \\ Q_n^m(\xi) \end{matrix}\right\} = (\xi^2-1)^{\frac{m}{2}} \frac{d^m \left\{\begin{matrix} P_n(\xi) \\ Q_n(\xi) \end{matrix}\right.}{d\xi^m} \qquad [18]$$

The exact solution of the present problem can be accomplished by an expansion of Φ in the associated Legendre polynomials [18]. The first term in the expansion is obviously equation [11]. The first step in such a procedure then consists of evaluating φ over the image ellipsoid by the expansion

$$\varphi_1 = \sum_{n,m} A_{nm} P_n^m\left[\mu(\mu', \xi' = \xi_0')\right] Q_n^m\left[\xi(\mu', \xi' = \xi_0')\right] \qquad [19]$$

and then determining the coefficients B_{nm} in the expansion for the first image in the image ellipsoid

$$\varphi_1' = -\sum_{n,m} B_{nm} P_n^m(\mu') Q_n^m(\xi' = \xi_0') \qquad [20]$$

so that the boundary condition [16] is satisfied. The effects and the rectification of the successive images are then evaluated by a similar process.

Although this method will lead to an exact solution, the extreme complexity of only the first term [11], after writing μ and ξ as functions of μ' and ξ', is a most convincing deterrent to proceeding with even the expansion [19]. Furthermore, the resulting expressions would

defeat the purpose, stated in the foregoing, of obtaining formulas that may be rapidly applied in engineering applications. As a result, the procedure that has been adopted leads to an approximate solution which approaches the exact solution in the limit as the ellipsoid recedes from the wall. This approximation is essentially an evaluation in a power series in the types [19] and [20] but with n=1 and m=0. A second approximation is also carried out based on an exact evaluation of image potentials in the neighborhood of the real ellipsoid but using only the first approximation in the rectification of these potentials.

THE APPROXIMATE SOLUTION

Starting with the solution of the flow about an ellipsoid in an infinite stream, equations [11] and [12], the potential function φ in the neighborhood of the image, assuming for the moment that the image is at rest, is, with the aid of [1'],

$$\varphi_1 = A\frac{\mu'\xi'}{\xi}\left\{\frac{1}{2}\ln\frac{\xi+1}{\xi-1} - 1\right\} \qquad [21]$$

Instead of evaluating φ_1 over the surface of the image, assume, instead, that the image lies entirely on a portion of the ellipsoidal surface confocal with the real ellipsoid*

---

* This method of approximation is somewhat analogous to the first steps in the solution given in Lamb's "Hydrodynamics" for the flow about two spheres. However, to

and which passes through the center of the image. The semi-minor diameter of this surface is $c\sqrt{\xi^2-1} = 2h$, so that, since $c=ae_o$,

$$\xi=\sqrt{1+\frac{4}{e_o^2}\left(\frac{h}{a}\right)^2}=\eta \quad \text{(say)} \qquad [22]$$

Therefore, the induced velocity potential due to the real ellipsoid is, approximately,

$$\Phi_1=A\mu'\xi'\left\{\frac{1}{2}\ln\frac{\eta+1}{\eta-1}-\frac{1}{\eta}\right\} \qquad [23]$$

This potential produces a normal velocity on the surface of the image proportional to

$$\frac{\partial\Phi_1}{\partial\xi'}=A\mu'\left\{\frac{1}{2}\ln\frac{\eta+1}{\eta-1}-\frac{1}{\eta}\right\} \qquad [24]$$

It is easily verified that the term [24] is cancelled by addition of the potential,

$$\Phi_1'=-A\mu'\left\{\frac{\frac{1}{2}\ln\frac{\eta+1}{\eta-1}-\frac{1}{\eta}}{\frac{1}{2}\ln\frac{1+e_o}{1-e_o}-\frac{e_o}{1-e_o^2}}\right\}\left\{\frac{1}{2}\xi'\ln\frac{\xi'+1}{\xi'-1}-1\right\} \qquad [25]$$

and that Φ_1' satisfies the equation of continuity [6].

---

the same degree of approximation, the present solution might be expected to give better comparative results, since the image ellipsoid "fits" the ellipsoidal surface confocal with the real ellipsoid better than the image sphere on the spherical surface concentric with the real sphere. Of course, as e approaches zero, this advantage disappears.

Equation [25] represents the potential of the first source image in the image ellipsoid.

Using the assumption [22], the potential φ_1', in the neighborhood of the real ellipsoid, takes on the value

$$\varphi_2' = -A\mu\xi \frac{\left\{\frac{1}{2}\ln\frac{\eta+1}{\eta-1} - \frac{1}{\eta}\right\}^2}{\left\{\frac{1}{2}\ln\frac{1+e_0}{1-e_0} - \frac{e_0}{1-e_0^2}\right\}} \qquad [26]$$

which, in turn is rectified by the potential

$$\varphi_2 = A\mu \left\{\frac{\frac{1}{2}\ln\frac{\eta+1}{\eta-1} - \frac{1}{\eta}}{\frac{1}{2}\ln\frac{1+e_0}{1-e_0} - \frac{e_0}{1-e_0^2}}\right\}^2 \left\{\frac{1}{2}\xi\ln\frac{\xi+1}{\xi-1} - 1\right\} \qquad [27]$$

The law of formation of the successive images is now clear. Remembering that an exactly similar process must be carried through starting with the image ellipsoid and holding the real ellipsoid at rest, the potential function for the entire flow, after evaluating all the images in the above manner is approximately

$$\Phi = \varphi + \varphi' = A\left\{\mu\left(\frac{1}{2}\xi\ln\frac{\xi+1}{\xi-1} - 1\right) + \mu'\left(\frac{1}{2}\xi'\ln\frac{\xi'+1}{\xi'-1} - 1\right)\right\} \sum_{\lambda=0}^{\infty} (-1)^{\lambda} \left(\frac{\frac{1}{2}\ln\frac{\eta+1}{\eta-1} - \frac{1}{\eta}}{\frac{1}{2}\ln\frac{1+e_0}{1-e_0} - \frac{e_0}{1-e_0^2}}\right)^{\lambda} \qquad [28]$$

The infinite power series in equation [28] converges absolutely if

$$\left|\frac{\frac{1}{2}\ln\frac{\eta+1}{\eta-1} - \frac{1}{\eta}}{\frac{1}{2}\ln\frac{1+e_0}{1-e_0} - \frac{e_0}{1-e_0^2}}\right| < 1$$

Since, from [22], $\eta^2 \geq 1$ for all values of h/a, and $0 \leq e_0 \leq 1$,

this condition requires that

$$\left|\frac{1}{3}\left(\frac{1}{\eta}\right)^3+\frac{1}{5}\left(\frac{1}{\eta}\right)^5+\frac{1}{7}\left(\frac{1}{\eta}\right)^7+\cdots\right|<\left|\frac{2}{3}e_o^3+\frac{4}{5}e_o^5+\frac{6}{7}e_o^7+\cdots\right| \qquad [29]$$

For the inequality [29] to be valid, it is sufficient to require only that $1/\eta < e_o$, or

$$1+\frac{4}{e_o^2}\left(\frac{h}{a}\right)^2 > \frac{1}{e_o^2}$$

so that the series converges absolutely for all values

$$\frac{h}{a} > \frac{1}{2}\sqrt{1-e_o^2} \qquad [30]$$

Furthermore, with this requirement, the solution [28] converges everywhere on all ellipsoids $0 \leq e_o \leq 1$ and everywhere in the field.

Finally, by using the formula for the sum of an absolutely convergent geometric series, and putting in the value of the constant, A, from equation [12], the solution may be written in closed form as

$$\Phi = -Uc\left\{\frac{\mu\left(\frac{1}{2}\xi \ln\frac{\xi+1}{\xi-1}-1\right)+\mu'\left(\frac{1}{2}\xi'\ln\frac{\xi'+1}{\xi'-1}-1\right)}{\frac{1}{2}\ln\left(\frac{\eta+1}{\eta-1}\right)\left(\frac{1+e_o}{1-e_o}\right)-\left(\frac{e_o}{1-e_o^2}-\frac{1}{\eta}\right)}\right\} \qquad [31]$$

THE FIRST APPROXIMATION TO THE PRESSURE DISTRIBUTION ON AN ELLIPSOID NEAR A WALL

Superposing a uniform velocity potential to transform the motion to one of flow past a stationary ellipsoid, the potential [31], to the same degree of approximation as the entire calculation so far, is

$$\Phi_1 = U\mu\left\{c\xi + B\left[\frac{1}{2}\,\xi \ln\left(\frac{\xi+1}{\xi-1}\right)\left(\frac{\eta+1}{\eta-1}\right) - \left(1+\frac{\xi}{\eta}\right)\right]\right\} \qquad [32]$$

where

$$B = -c\left[\frac{1}{2}\ln\left(\frac{\eta+1}{\eta-1}\right)\left(\frac{1+e_0}{1-e_0}\right) - \left(\frac{e_0}{1-e_0^2}+\frac{1}{\eta}\right)\right]^{-1} \qquad [33]$$

The velocity components in the neighborhood of the real ellipsoid are, from [5]

$$\left.\begin{aligned}
\frac{u_\mu}{U} &= -\sqrt{\frac{1-\mu^2}{\xi^2-\mu^2}}\left\{\xi + \frac{B}{c}\left[\frac{1}{2}\,\xi\ln\left(\frac{\xi+1}{\xi-1}\right)\left(\frac{\eta+1}{\eta-1}\right) - \left(1-\frac{\xi}{\eta}\right)\right]\right\} \\
\frac{u_\xi}{U} &= -\sqrt{\frac{\xi^2-1}{\xi^2-\mu^2}}\left\{1 + \frac{B}{c}\left[\frac{1}{2}\ln\left(\frac{\xi+1}{\xi-1}\right)\left(\frac{\eta+1}{\eta-1}\right) - \left(\frac{\xi}{\xi^2-1}+\frac{1}{\eta}\right)\right]\right\} \\
\frac{u_\omega}{U} &= 0
\end{aligned}\right\} \qquad [34]$$

The fact that this approximation gives a symmetric velocity field is a direct result of expansion in a series of $P_1(\mu)Q_1(\xi)$, and, thus, cannot be expected to predict a difference in velocity distributions between points on opposite sides of the ellipsoid. Nevertheless, these velocities may be expected to give an approximately correct average distribution over the entire surface. Since the images are evaluated at the center of the ellipsoid, neglecting the variations between this point and points on the ellipsoidal surface, and these values then applied to every point on the surface, this solution will evidently underestimate the effects near the center and overestimate

toward the two ends. From another point of view, that this is the case can be seen from the fact that the expansion of the images by approximations of the type [23] is equivalent to a rectilinear flow, which evidently give velocities that are too low at the center and too high at the leading and trailing ends. In general, it might be expected that equations [34] will most closely approximate the velocity distribution along the meridian parallel to the wall.

Evaluating equations [34] on the surface of the ellipsoid, $\xi_o = 1/e_o$, and putting $\mu = x/c\ \xi_o = x/a$, only the tangential component remains:

$$\left.\frac{u_\mu}{U}\right|_{\xi=\frac{1}{e_o}} = -\frac{B}{a}\left(\frac{e_o^2}{1-e_o^2}\right)\sqrt{\frac{1-\left(\frac{x}{a}\right)^2}{1-e_o^2\left(\frac{x}{a}\right)^2}} \qquad [34']$$

To this degree of approximation, then, the pressure distribution, in non-dimensional form, is

$$\frac{p-p_\infty}{\frac{1}{2}\rho U^2} = 1 - \left\{\frac{1-\left(\frac{x}{a}\right)^2}{1-e_o^2\left(\frac{x}{a}\right)^2}\right\}\left\{\frac{\frac{e_o^2}{1-e_o^2}}{\frac{1}{2e_o}\ln\left(\frac{\eta+1}{\eta-1}\right)\left(\frac{1+e_o}{1-e_o}\right)-\left(\frac{1}{1-e_o^2}+\frac{1}{e_o\eta}\right)}\right\}^2 \qquad [35]$$

where p is the pressure at the surface of the ellipsoid,

p_∞ is the pressure in the undisturbed stream, and

ρ is the mass density of the fluid.

From the geometry of the ellipsoid, it is readily shown that

$$\frac{1-\left(\frac{x}{a}\right)^2}{1-e_o^2\left(\frac{x}{a}\right)^2}=\sin^2\theta$$

where θ is the angle between the normal to the surface of the ellipsoid and the direction of motion. As $\eta \longrightarrow \infty$, equation [35] reduces to the familiar result for an ellipsoid in an infinite stream:

$$\frac{P-P_\infty}{\frac{1}{2}\rho U^2}=1-\frac{A^2\sin^2\theta}{U^2a^2}\left(\frac{e_o^2}{1-e_o^2}\right)^2 \qquad [36]$$

The pressure distributions for ellipsoids with ratios of a/b = 4 and a/b = 6 at various distances h/2b from the wall are shown in Figures 2 and 3. It is seen that for these forms the wall effect may be neglected for distances greater than about three diameters(i.e. for h/2b greater than 3). By rewriting equation [35] in the form

$$\frac{P-P_\infty}{\frac{1}{2}\rho U^2}=1-C\sin^2\theta \qquad [35']$$

and plotting C as a function of h/2b, with a/b as parameter, Figure 4, the distances beyond which the wall effect may be neglected can be quickly estimated.

A SECOND APPROXIMATION TO THE PRESSURE DISTRIBUTION

For reasons already pointed out in the foregoing, the above approximation cannot be used for applications in which it is desired to obtain a measure of the difference in pressures on opposite sides of the model. To obviate this shortcoming, the solution [31] will be evaluated

in a more exact manner than the approximation [32]. Although the following evaluation is not completely justified on the basis of the approximations used in the calculation of equation [31], nevertheless, the result will be correct to at least the same order as the first part of the exact expansion suggested in equations [19] and [20]. This proposal consists essentially of an exact evaluation in equation [31] of the image potentials of the image ellipsoid in the neighborhood of the real ellipsoid while evaluating the successive rectifying images by the approximation $\xi' = \eta, \mu' = \mu\,\xi/\eta$.

For this purpose, as well as for computations of pressures in the surrounding fluid, it will be more convenient to express Φ, equation [31], in cartesian coordinates. Rewriting equation [2] as a quadratic in ξ^2, this equation becomes

$$\xi^4 - \xi^2\left[1+\left(\frac{x}{c}\right)^2+\left(\frac{y}{c}\right)^2+\left(\frac{z}{c}\right)^2\right]+\left(\frac{x}{c}\right)^2 = 0 \qquad [37]$$

since $\bar{y}^2 = y^2 + z^2$; and, solving for ξ^2,

$$\xi^2 = \frac{1}{2}\left[1+\left(\frac{x}{c}\right)^2+\left(\frac{y}{c}\right)^2+\left(\frac{z}{c}\right)^2\right]+\frac{1}{2}\sqrt{\left[1+\left(\frac{x}{c}\right)^2+\left(\frac{y}{c}\right)^2+\left(\frac{z}{c}\right)^2\right]^2-4\left(\frac{x}{c}\right)^2} \qquad [38]$$

where the positive sign has been taken before the radical to exclude the imaginary ellipsoids between $\pm c$. The value of ξ in cartesian coordinates is, thus,

$$\xi = \sqrt{\frac{1}{2}\left\{\left[1+\left(\frac{x}{c}\right)^2+\left(\frac{y}{c}\right)^2+\left(\frac{z}{c}\right)^2\right]+\sqrt{\left[1+\left(\frac{x}{c}\right)^2+\left(\frac{y}{c}\right)^2+\left(\frac{z}{c}\right)^2\right]^2-4\left(\frac{x}{c}\right)^2}\right\}} \qquad [39]$$

since ξ takes on only positive values.

Similarly, from equations [3] and [13], and putting $\bar{y}$ in terms of y and z, ξ' expressed in cartesian coordinates is

$$\xi' = \sqrt{\frac{1}{2}\left\{\left[1+\left(\frac{x}{c}\right)^2+\left(\frac{y}{c}\right)^2+\left(\frac{z}{c}\right)^2+4\left(\frac{h}{c}\right)^2-4\frac{hy}{c^2}\right]+\sqrt{\left[1+\left(\frac{x}{c}\right)^2+\left(\frac{y}{c}\right)^2+\left(\frac{z}{c}\right)^2+4\left(\frac{h}{c}\right)^2-4\frac{hy}{c^2}\right]^2-4\left(\frac{x}{c}\right)^2}\right\}} \qquad [40]$$

The expressions for μ and μ' are obtained directly from equations [1'], [39] and [40].

Let

$$\alpha = 1+\left(\frac{x}{c}\right)^2+\left(\frac{y}{c}\right)^2+\left(\frac{z}{c}\right)^2 \qquad [41]$$

$$\beta = \sqrt{\alpha^2-4\left(\frac{x}{c}\right)^2} \qquad [42]$$

$$\gamma = \alpha+4\left(\frac{h}{c}\right)^2-4\frac{hy}{c^2} \qquad [43]$$

$$\zeta = \sqrt{\gamma^2-4\left(\frac{x}{c}\right)^2} \qquad [44]$$

With this notation,

$$\xi = \sqrt{\frac{\alpha+\beta}{2}} \qquad [45]$$

$$\xi' = \sqrt{\frac{\gamma+\zeta}{2}} \qquad [46]$$

and the equation of the potential becomes

$$\Phi_2 = Ux+BU\frac{x}{c}\left\{\frac{1}{2}\ln\left(\frac{\xi+1}{\xi-1}\right)\left(\frac{\xi'+1}{\xi'-1}\right)-\left(\frac{1}{\xi}+\frac{1}{\xi'}\right)\right\} \qquad [47]$$

The velocity components in the directions of increasing x, y and z are, then,

$$\frac{u_x}{U} = -\frac{1}{U}\frac{\partial \Phi_2}{\partial x} = -1 - \frac{B}{c}\left\{\frac{1}{2}\ln\left(\frac{\xi+1}{\xi-1}\right)\left(\frac{\xi'+1}{\xi'-1}\right) - \left(\frac{x}{c}\right)^2\left(\frac{1}{\beta\xi^3} + \frac{1}{\zeta\xi'^3}\right) - \left(\frac{1}{\xi} + \frac{1}{\xi'}\right)\right\} \quad [48]$$

$$\frac{u_y}{U} = -\frac{1}{U}\frac{\partial \Phi_2}{\partial y} = \frac{B}{c}\left(\frac{x}{c}\right)\left\{\frac{y}{c}\left[\beta\left(\xi^3 - \xi\right)\right]^{-1} + \left(\frac{y}{c} - 2\frac{h}{c}\right)\left[\zeta\left(\xi'^3 - \xi'\right)\right]^{-1}\right\} \quad [49]$$

$$\frac{u_z}{U} = -\frac{1}{U}\frac{\partial \Phi_2}{\partial z} = \frac{B}{c}\left(\frac{x}{c}\right)\left(\frac{z}{c}\right)\left\{\left[\beta\left(\xi^3 - \xi\right)\right]^{-1} + \left[\zeta\left(\xi'^3 - \xi'\right)\right]^{-1}\right\} \quad [50]$$

The pressure at any point is then

$$\frac{p - p_\infty}{\frac{1}{2}\rho U^2} = 1 - \left\{\left(\frac{u_x}{U}\right)^2 + \left(\frac{u_y}{U}\right)^2 + \left(\frac{u_z}{U}\right)^2\right\} \quad [51]$$

To calculate the pressure distribution on any ellipsoidal surface confocal with the real ellipsoid, it is only necessary to replace ξ by 1/e where e is the eccentricity of the confocal ellipsoid. In addition, the values of α and β reduce to

$$\alpha_{\xi=\frac{1}{e}} = \frac{1}{e^2} + \left(\frac{x}{a}\right)^2$$

and

$$\beta_{\xi=\frac{1}{e}} = \frac{1}{e^2} - \left(\frac{x}{a}\right)^2$$

Otherwise, the substitutions [41] through [44] must be used. For any point on the wall, put y=h, $\gamma=\alpha$, $\zeta=\beta$, $\xi=\xi'$, in the formulas [48] through [50], so that, on the wall,

$$\left.\begin{aligned} \frac{u_x}{U}\bigg|_{y=h} &= -1 - \frac{B}{c}\left\{\frac{1}{2}\ln\frac{\xi+1}{\xi-1} - \frac{2}{\beta\xi^3}\left(\frac{x}{c}\right)^2 - \frac{2}{\xi}\right\} \\ \frac{u_y}{U}\bigg|_{y=h} &= 0 \\ \frac{u_z}{U}\bigg|_{y=h} &= 2\frac{B}{c}\left(\frac{x}{c}\right)\left(\frac{z}{c}\right)\left[\beta\left(\xi^3 - \xi\right)\right]^{-1} \end{aligned}\right\} \quad [52]$$

The pressure distributions on three half-meridians of an ellipsoid with a ratio a/b=4 at a distance of one diameter from the wall are shown in Figure 5. It is seen that the solution correctly predicts a difference of pressure on opposite sides of the ellipsoid, and that the first approximation represents most closely the pressure distribution on the meridian parallel to the wall. The most interesting results are the prediction, near the leading and trailing ends, of a pressure increase over that of the single ellipsoid in a fluid of infinite extent, and the prediction, near these ends, of pressures on the meridian closest to the wall that are higher than those on the meridian farthest from the wall.* It is also of interest that for this case this solution shows a difference as high as 15 per cent between the minimum pressures on the meridians closest and farthest from the wall. A comparison of the two approximations on the circumference of two stations on the ellipsoid at a distance of one diameter from the wall is shown in Figure 6.

To check the accuracy of the solution, pressure distributions corresponding to the computations of Figures 2, 3, and 5 were measured on two ellipsoid models. These

---

*

The solution also predicts the displacement of the stagnation points. However, this change is so small as to be indiscernable on a graph, and, as a matter of fact, was well within the experimental error of the tests conducted to check the solution.

experiments are discussed in succeeding sections.

THE EXPERIMENTAL ARRANGEMENT, MODELS, AND TECHNIQUE OF MEASUREMENT

To facilitate the experimental work, it was decided to construct models, which, though they deviated at the center sections by very slight amounts from true ellipsoids, could easily be adapted to equipment standard in the Hydrodynamics Laboratory. This necessitated the use of a straight cylindrical middlebody over 7.5 per cent of the 4:1 ellipsoid and 5 per cent of the 6:1 ellipsoid. The principal dimensions and the location of the piezometers for the models are shown in Figure 7. The lengths of the models were adjusted so that the coordinates would match the dimensions of the middlebody at the stations of contact. Although the fineness ratios are increased by negligible amounts, the disadvantage of the construction was the introduction of discontinuities in the slopes and curvatures of the surface at the points of contact. Although this condition gave resulting local deviations in the pressure measurements, it apparently had little or no effect on the pressure distribution as a whole.

A photograph of the models illustrating the method of assembly for the tests is shown in Figure 8. The nose and afterbody sections, which were secured to the middlebody with an internal stud, could be rotated about the

major axis, and the entire assembly rotated about the vertical minor axis on a spindle within the shield. The method of communicating pressures from the piezometers through rubber and then brass tubing of very small diameter up through the spindle is standard in the Hydrodynamics Laboratory.

The experiments were conducted in the free surface flume (4) in this laboratory. A photograph of the experimental arrangement is shown in Figure 9 and, the various components are identified in Figure 10. The pressure leads are carried out through the shield and fairwater to a manifold communicating with a water manometer open to the atmosphere. The use of the vacuum pump and overhead reservoir in bleeding the manometric system and in accelerating the change in level of the fluid in the manometer when seeking equilibrium (a device necessitated by the small internal diameters of the pressure leads) are clear.

To simulate the effect of the wall, a plate was installed below the model on a strut constructed in sections so that the distance from the surface of the plate to the horizontal meridian of the model could be varied. Although the width of the plate was limited to avoid damage to the lucite walls of the flume, the ratio of width of plate to model diameter was large enough so that the effects of "leakage" through the gap could be safely neglected. In

addition, the model was supported well downstream from the leading edge of the plate to insure the establishment of the wall effect; nevertheless, the distortion of the parallel flow due to growth of the boundary layer on the plate was insignificant for this distance.

A measure of the velocity head was obtained on a similar open manometer from a point on the upstream riser of the flume. Referring to Figure 10, it is clear that the pressure coefficient is

$$\frac{p-p_\infty}{\frac{1}{2}\rho U^2} = \frac{h_p - h_o}{h_v - h_o} \qquad [53]$$

where h_o is the depth of water in the flume,

h_p is the indicated pressure head at a piezometer referred to the floor of the flume, and

h_v is the indicated total head* at the model referred to the floor of the flume.

Preliminary experiments to determine the accuracy of the measurements and the effect of the cylindrical middlebody were made with the 4:1 ellipsoid model without the effects of the plate. The source of the largest errors lies in the method of alignment of the model in yaw. This alignment was accomplished by measurements from the side of the channel to the leading and trailing ends of the

---

* In the actual experiment, the difference $h_v - h_o$ was calibrated against the correct velocity head at the model.

model, with the resultant errors in angular setting due to the short distance between the points of measurement. To determine the effect of this error, pressure distributions were taken over the model with three independent settings of the zero yaw position. Although no pressure measurements could be taken along the half-meridian farthest from the bottom of the channel because of the effect of the shield, readings were taken along the half-meridian closest to the channel floor and on the horizontal meridian of the model. The latter measurements were first made on one side of the model; the model was then rotated 180 degrees about its major axis and the readings repeated on this opposite side without altering the setting in yaw. This experiment also served as an indication of the shield effect at this position.

The results of the preliminary experiments are shown in Figure 11. It is seen that the pressure distribution along the half-meridian closest to the channel bottom was unaffected by the small errors in the angle of yaw. On the other hand, the measurements along the horizontal meridian show a rather large deviation from those along the vertical half-meridian. However, the arithmetic averages of the measurements along the horizontal half-meridian fall quite nicely on those along the vertical meridian for the errors in yaw within which the model could be set. As a result,

this technique of rotating the model and averaging the readings on the horizontal half-meridians was used throughout the remaining program. That these average readings evidently gave the correct pressure distribution indicates that the shield had no measureable effect as far away as the horizontal meridian. It may also be seen that pressures in the vicinity of the cylindrical middle section show somewhat more scatter than the other data, indicating a local region of separation and, consequently, unstable flow.

RESULTS OF THE PRESSURE MEASUREMENTS

All tests were made at a Reynolds number,

$$R_e = \frac{U(2b)}{\nu} = 2.5 \times 10^5$$

where ν is the kinematic viscosity. Although this Reynolds number is slightly less than the Reynolds number (defined on the same basis) required for transition in the boundary layer on forms of similar shape and fineness ratio (see e.g. (17)), the effects of laminar separation and transition on the pressure distribution are confined to a small region of the after end. As a result, the measured and theoretical pressure distributions should be in good agreement over at least 75 per cent of the length with the major defect occurring near the very end of the model. Consequently, the deviation of the data from the theoretical curve for the ellip-

soid without wall effect, Figure 11, is probably due to other sources. The accuracy of construction of the models was such as to exclude deviations as large as those shown. However, in reducing the data by the formula [53], no corrections were made for any pressure excess that might have been present at the position of the model due to residual curvature of the stream induced in leaving the nozzle. An idea of how small the curvature (or how large the radius of curvature) can be in order to make the measured and theoretical data coincide at the point of minimum pressure can be obtained from a short computation. The pressure gradient in the direction of increasing pressure is

$$\frac{\partial p}{\partial r} = \rho \frac{u^2}{r}$$

or, approximately,

$$\frac{\Delta p}{\frac{1}{2}\rho U^2} = 2\frac{R}{r}$$

where r is the radius of curvature and R is the distance of the model below the water surface. The difference in pressure coefficient required for coincidence at the minimum point is 0.005, so that for the model at a depth of 9 inches, the radius of curvature would be 300 feet - large enough so that it could not be detected from measurements of the free surface level. However, for purposes of comparison with the theoretical computations, and since the

presence of the plate would tend to reduce this correction, it was considered sufficient to use the data directly as obtained from formula [53].

The data for the 6:1 ellipsoid taken without the presence of the plate show the same trends, but with somewhat more scatter in the vicinity of the middlebody, (Figure 17).

The majority of the measurements were made with the 4:1 ellipsoid model. In addition to the tests without the plate, runs were made with the model at distances from centerline to plate surface of 3.0, 2.0, 1.5, 1.0, and 0.75 diameters. Since it was anticipated that the differences between the pressures on the half-meridian closest to the plate and the meridian parallel to the plate would be small for distances of 3.0, 2.0, and 1.5 diameters, the pressure distributions for these cases were measured only along the closest half-meridian. At the remaining two distances, the pressures were measured along both of these lines. Measurements on the 6:1 ellipsoid were made only without the plate and at a distance of one diameter from the plate.

The results of the experiments are shown on Figures 11 through 18 in the order outlined above. In all cases, the distributions are very nearly symmetric with respect to the transverse vertical plane through the center of the

model except near the trailing ends where the effects of separation result in the pressure defect.

From Figure 12, it is seen that the measured pressure distribution lies very close to that calculated from the first approximation for h/2b=3.0. Since, from Figure 2, the pressure distribution at this distance coincides with that for an infinite stream (for the scale of ordinates used), the agreement of data indicates that the presence of the plate does tend to reduce the curvature of the stream and, therefore, the pressure excess at the position of the model.

The rather large scatter of the data obtained near the middlebody, for both models at the shorter separations from the plate, is probably due to the discontinuities in slopes and curvatures mentioned above. However, for purposes of comparison with the theoretical values, this shortcoming is not serious, since the minimum points could evidently be determined with sufficient accuracy by careful fairing of the data on either side of this position.

COMPARISON OF THE MEASURED AND CALCULATED PRESSURE DISTRIBUTIONS

For purposes of comparison, the pressure distributions computed by the first approximation are plotted together with the measured data on Figures 12 through 18. The conclusion reached in the foregoing that, for this approximation, the computed values would be underestimated near the center of the model and overestimated at the leading and trailing ends

is clearly borne out in all cases. The computations and the measured values begin to show fairly large deviations at the distance of two diameters. In this case, the deviation at the point of minimum pressure is approximately 4 per cent for the distribution along the half-meridian closest to the plate. For smaller separations of model and plate, the deviation increases rapidly with an error of about 14.6 per cent at the distance of one diameter and 25 per cent at 0.75 diameter (1/4 diameter separation). Although these errors are large for the half-meridian closest to the wall, this approximation will be somewhat better for positions on the ellipsoid farther from the wall.

For the 6:1 ellipsoid, the deviation of the first approximation from the minimum value on the meridian closest to the wall for a distance of one diameter is also about 15 per cent, with somewhat better agreement along the horizontal meridian.

The data for the 4:1 ellipsoid at a distance of one diameter from the plate are compared in Figure 19 with the corresponding pressure distributions obtained from the second approximation. Except for the anomalous data near the center of the model, the computed and measured values along the horizontal meridian show excellent agreement. On the other hand, the deviation of the calculations from the faired curve for the minimum point on the vertical mer-

idian is about 6 per cent.

Since the largest errors may be expected to occur at the point of minimum pressure on the meridian closest to the wall, the computed and measured data are compared on this basis; the results are tabulated in Table I (page 33) for all the measurements. The percentage deviations of the first approximation appear to vary consistently. However, for the small differences of measured values and data computed by the second approximation, the error is largely dependent on the method of fairing. The fact that the direction of the error changes for the two larger separations indicates that these percentages are too high and that the deviations shown for the smaller separations are probably somewhat too low. The deviation for the 6:1 ellipsoid for the one case compared is of the same order as that for the 4:1 ellipsoid.

CONCLUDING REMARKS ON THE ACCURACY AND APPLICABILITY OF THE TWO APPROXIMATIONS

In general, the agreement between measured data and that computed by the second approximation is better than might have been expected. This result indicates that the successive images in an exact solution lessen in strength quite rapidly beyond the first image. The expansion developed herein, equation [28], also exhibits this property for large values of the eccentricity, e_o, so that the solution

TABLE I

COMPARISON OF MEASURED AND COMPUTED VALUES OF THE MINIMUM PRESSURE COEFFICIENTS (x/a=0) ON THE HALF-MERIDIAN CLOSEST TO THE WALL

Ellipsoid Model	Distance From Wall in Diameters	Measured (Faired) Values	First Approximation Equation [35]	
	h/2b	$\frac{p-p_\infty}{\frac{1}{2}\rho U^2}$	$\frac{p-p_\infty}{\frac{1}{2}\rho U^2}$	Percent Deviation
4:1	0.75	-0.295	-0.221	-25
	1.0	-0.233	-0.199	-14.6
	1.5	-0.201	-0.181	- 9
	2.0	-0.182	-0.175	- 4
	∞	--	-0.1707	--
6:1	1.0	-0.145	-0.123	-15

Ellipsoid Model	Distance From Wall in Diameters	Measured (Faired) Values	Second Approximation Equation [51]	
	h/2b	$\frac{p-p_\infty}{\frac{1}{2}\rho U^2}$	$\frac{p-p_\infty}{\frac{1}{2}\rho U^2}$	Percent Deviation
4:1	0.75	-0.295	-0.264	-10.5
	1.0	-0.233	-0.219	- 6
	1.5	-0.201	-0.207	+ 3
	2.0	-0.182	-0.178	+ 2.2
	∞	--	-0.1707	--
6:1	1.0	-0.145	-0.137	- 5.5

can be expected to give even better results for fineness ratios larger than those of the ellipsoids tested. (The latter result was anticipated in the formulation of the approximation used.)

From the results of Table I, it appears that the second approximation, equation [51], may be used with good accuracy for ellipsoids even as close as one diameter from its center to the wall. The largest error will occur at the point of minimum pressure on the meridian closest to the wall with errors smaller than those shown in Table I for other points of the surface. On the other hand, the usefulness of the first approximation is apparently limited to checks of the type shown in Figure 4 on the existence of wall effect and to calculations of pressure distributions along the meridian that is parallel to the wall. The simplicity of this approximation, equation [35], especially recommends it where a rapid calculation is wanted of the change in pressure distribution for varying separations, and where a high degree of precision in actual values is not required. For points near the center of the meridian parallel to the wall, however, the first approximation approaches in accuracy the results of the second approximation.

For convenience in use the more important results are summarized in the Appendix.

REFERENCES

1. Mumma, Lt. Comdr. A. G., "The Variable Pressure Water Tunnels at the David W. Taylor Model Basin", Trans. Soc. of Naval Arch. and Marine Eng., Vol. 49, 1941.

2. Daily, James W., "The Water Tunnel as a Tool in Hydraulic Research", Proc. Third Hydr. Conf., Bull. 31, Univ. of Iowa Studies in Engineering, 1947.

3. Rupp, Comdr. L. A.,"Cavitation Tunnels in Foreign Model Basin and Research Institutions", U. S. Naval Technical Mission in Europe Report No. 534-45, 1945. (Distributed by Supt. of Documents, Wash., D. C.)

4. Knapp, Robert T.; Levy, Joseph; O'Neill, J. Pat; Brown, F. Barton; "The Hydrodynamics Laboratory of the California Institute of Technology", Presented at sessions of the Hydraulics Division, A.S.M.E. Annual Meeting, Dec. 2, 1947.

5. Knapp, R. T., and Hollander, A., "Laboratory Investigations of the Mechanism of Cavitation", Presented at sessions of the Hydraulics Division, A.S.M.E. Annual Meeting, Dec. 2, 1947.

6. Eisenberg, P., "A Cavitation Method for the Development of Forms Having Specified Critical Cavitation Numbers", David Taylor Model Basin Report No. 647, Sept., 1947.

7. Durand, W. F., "Aerodynamic Theory", Vol. III, Div. I, Part 1, pp. 280 - 319, Julius Springer, Berlin, 1935.

8. Stewart, H. J., "The Effect of Wind Tunnel Wall Interference on the Stalling Characteristics of Wings", Jour. Aero. Sci., Sept., 1941,
----, "A Correction to the Yawing Moment Due to Ailerons for Circular Wind Tunnels", Jour. Aero. Sci., June, 1939.

9. Lock, M., "The Interference of a Wind Tunnel on a Symmetrical Body", British A.R.C., Rep. and Memo. 1275, 1929.

10. Lock, C. N. H., and Johansen, F. C., "Wind Tunnel Interference on Streamline Bodies", Rep. and Memo. 1451, 1931.

11. Lamb, H., "Hydrodynamics", Sixth Edition, pg. 139 - 143, Cambridge Univ. Press, London, 1932.

12. Durand, W. F., "Aerodynamic Theory", Vol. I, Div. C, pg. 277, Julius Springer, Berlin, 1934.

13. Whittaker, E. T., and Watson, G. N., "A Course in Modern Analysis", Fourth Edition, pg. 317 - 319, Cambridge Univ. Press, London, 1927.

14. Lamb, H., loc. cit., pg. 114.

15. Smythe, W. R., "Static and Dynamic Electricity", McGraw-Hill Book Comp., New York, 1939.

16. Whittaker, E. T., and Watson, G. N., loc. cit., pg. 323 - 326.

17. Freeman, Hugh B., "Measurements of Flow in the Boundary Layer of a 1/40-Scale Model of the U. S. Airship 'Akron'", N.A.C.A. Report No. 430, 1932.

APPENDIX

SUMMARY OF FORMULAS

Notation

a - semi-major axis of the ellipsoid

b - semi-minor axis of the ellipsoid

c - x-coordinate of the focus of the ellipsoid

e - eccentricity of a confocal ellipsoidal surface

e_o - eccentricity of the ellipsoid

h - distance from center of the ellipsoid to the wall

p - pressure at a point in the field

p_∞ - pressure in the undisturbed fluid

ρ - mass density of the fluid

θ - angle between normal to the ellipsoid and the direction of motion

U - velocity of the undisturbed fluid

u_μ - tangential component of velocity along an ellipsoidal surface in any meridianal plane

u_ξ - normal component of velocity along an ellipsoidal surface

u_ω - tangential component of velocity along an ellipsoidal surface perpendicular to any meridianal plane

u_x, u_y, u_z - velocity components in the direction of the cartesian coordinates

x, y, z - cartesian coordinates in coordinate system of the real ellipsoid

μ, ξ, ω - ovary ellipsoidal coordinates in coordinate system of the real ellipsoid

μ', ξ', ω' - ovary ellipsoidal coordinates in coordinate system of the image ellipsoid

$$\alpha = 1 + \left(\frac{x}{c}\right)^2 + \left(\frac{y}{c}\right)^2 + \left(\frac{z}{c}\right)^2 \qquad [41]$$

$$\beta = \sqrt{\alpha^2 - 4\left(\frac{x}{c}\right)^2} \qquad [42]$$

$$\gamma = \alpha + 4\left(\frac{h}{c}\right)^2 - 4\frac{hy}{c^2} \qquad [43]$$

$$\zeta = \sqrt{\gamma^2 - 4\left(\frac{x}{c}\right)^2} \qquad [44]$$

$$\xi = \sqrt{\frac{\alpha+\beta}{2}} \qquad [45]$$

$$\xi' = \sqrt{\frac{\gamma+\zeta}{2}} \qquad [46]$$

$$\eta = \sqrt{1 + \frac{4}{e_o^2}\left(\frac{h}{a}\right)^2} \qquad [47]$$

Pressure Distribution on an Ellipsoid in an Infinite Stream:

$$\frac{P-P_\infty}{\frac{1}{2}\rho U^2} = 1 - \frac{A^2 \sin^2\theta}{U^2 a^2}\left(\frac{e_o^2}{1-e_o^2}\right)^2 \qquad [36]$$

where

$$A = \frac{Uc}{\frac{e_o}{1-e_o^2} - \frac{1}{2}\ln\frac{1+e_o}{1-e_o}} \qquad [12]$$

Pressure Distribution on an Ellipsoid Near a Plane Wall -- First Approximation:

$$\frac{P-P_\infty}{\frac{1}{2}\rho U^2} = 1 - C\sin^2\theta \qquad [35']$$

where

$$C = \left\{ \frac{\frac{e_o^2}{1-e_o^2}}{\frac{1}{2e_o} \ln\left(\frac{\eta+1}{\eta-1}\right)\left(\frac{1+e_o}{1-e_o}\right) - \left(\frac{1}{1-e_o^2} + \frac{1}{e_o \eta}\right)} \right\}$$

and

$$\sin^2\theta = \frac{1-\left(\frac{x}{a}\right)^2}{1-e_o^2\left(\frac{x}{a}\right)^2}$$

Pressure Distribution at Any Position in the Field -- Second Approximation:

$$\frac{u_x}{U} = -1 - \frac{B}{c}\left\{\frac{1}{2}\ln\left(\frac{\xi+1}{\xi-1}\right)\left(\frac{\xi'+1}{\xi'-1}\right) - \left(\frac{x}{c}\right)^2\left(\frac{1}{\beta\xi^3} + \frac{1}{\zeta\xi'^3}\right) - \left(\frac{1}{\xi} + \frac{1}{\xi'}\right)\right\} \qquad [48]$$

$$\frac{u_y}{U} = \frac{B}{c}\left(\frac{x}{c}\right)\left\{\frac{y}{c}\left[\beta(\xi^3-\xi)\right]^{-1} + \left(\frac{y}{c} - 2\frac{h}{c}\right)\left[\zeta(\xi'^3-\xi')\right]^{-1}\right\} \qquad [49]$$

$$\frac{u_z}{U} = \frac{B}{c}\left(\frac{x}{c}\right)\left(\frac{z}{c}\right)\left\{\left[\beta(\xi^3-\xi)\right]^{-1} + \left[\zeta(\xi'^3-\xi)\right]^{-1}\right\} \qquad [50]$$

where $B = -c\left[\frac{1}{2}\ln\left(\frac{\eta+1}{\eta-1}\right)\left(\frac{1+e_o}{1-e_o}\right) - \left(\frac{e_o}{1-e_o^2} + \frac{1}{\eta}\right)\right]^{-1}$ [33]

$$\frac{p-p_\infty}{\frac{1}{2}\rho U^2} = 1 - \left\{\left(\frac{u_x}{U}\right)^2 + \left(\frac{u_y}{U}\right)^2 + \left(\frac{u_z}{U}\right)^2\right\} \qquad [51]$$

Pressure Distribution on Any Ellipsoidal Surface -- Second Approximation:

In formulas [48], [49], [50], and [51] above, put

$$\xi = \frac{1}{e}$$

$$\alpha = \frac{1}{e^2} + \left(\frac{x}{a}\right)^2$$

$$\beta = \frac{1}{e^2} - \left(\frac{x}{a}\right)^2$$

Pressure Distribution at Any Point on the Wall:

$$\left.\begin{aligned} \frac{u_x}{U} &= -1 - \frac{B}{c}\left\{\ln\frac{\xi+1}{\xi-1} - \frac{2}{\beta\xi^3}\left(\frac{x}{c}\right)^2 - \frac{2}{\xi}\right\} \\ \frac{u_y}{U} &= 0 \\ \frac{u_z}{U} &= 2\frac{B}{c}\left(\frac{x}{c}\right)\left(\frac{z}{c}\right)\left[\beta(\xi^3-\xi)\right]^{-1} \end{aligned}\right\} \qquad [52]$$

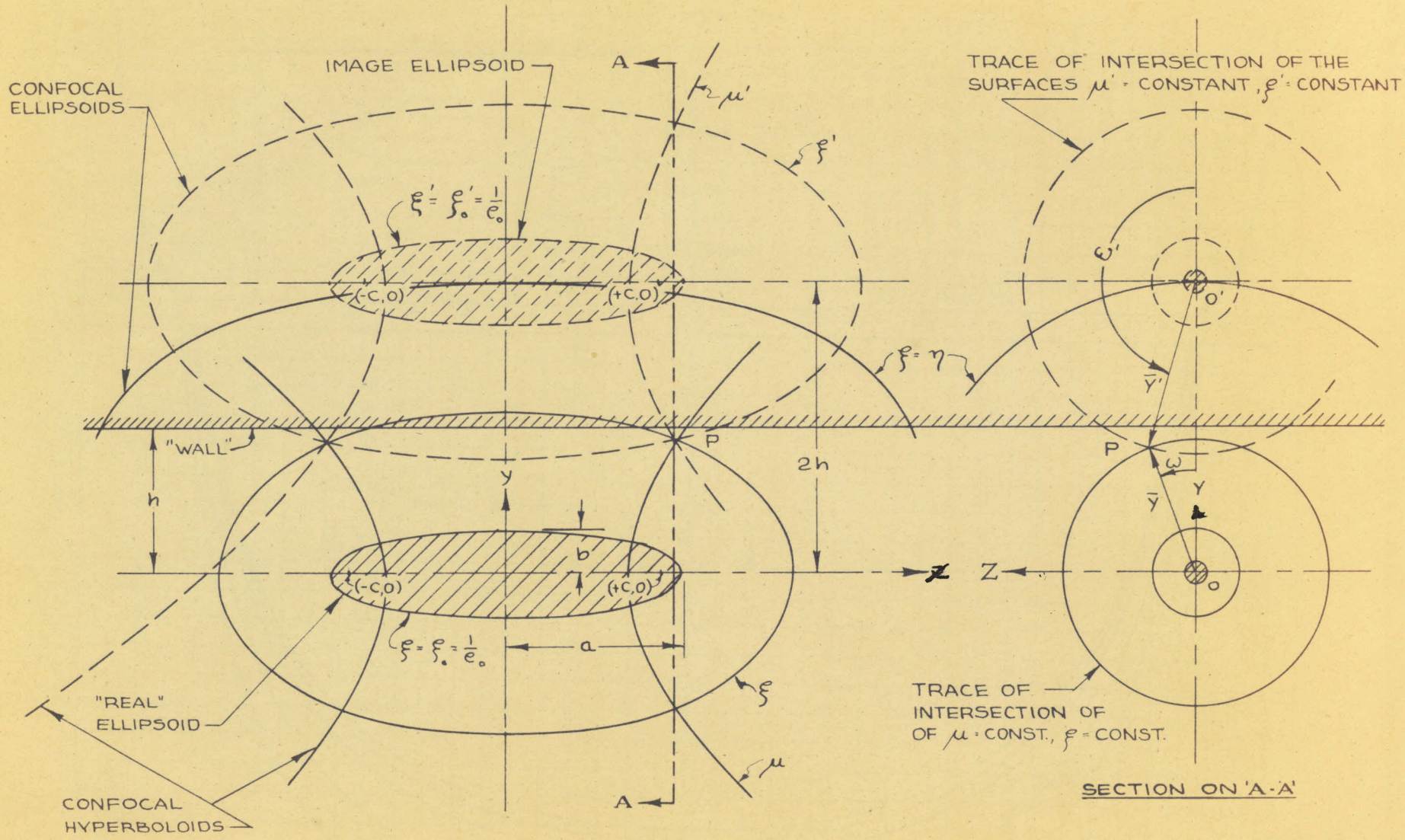

FIGURE 1

FIGURE 1
MODEL FOR THE CALCULATION OF FLOW ABOUT AN ELLIPSOID NEAR A PLANE WALL

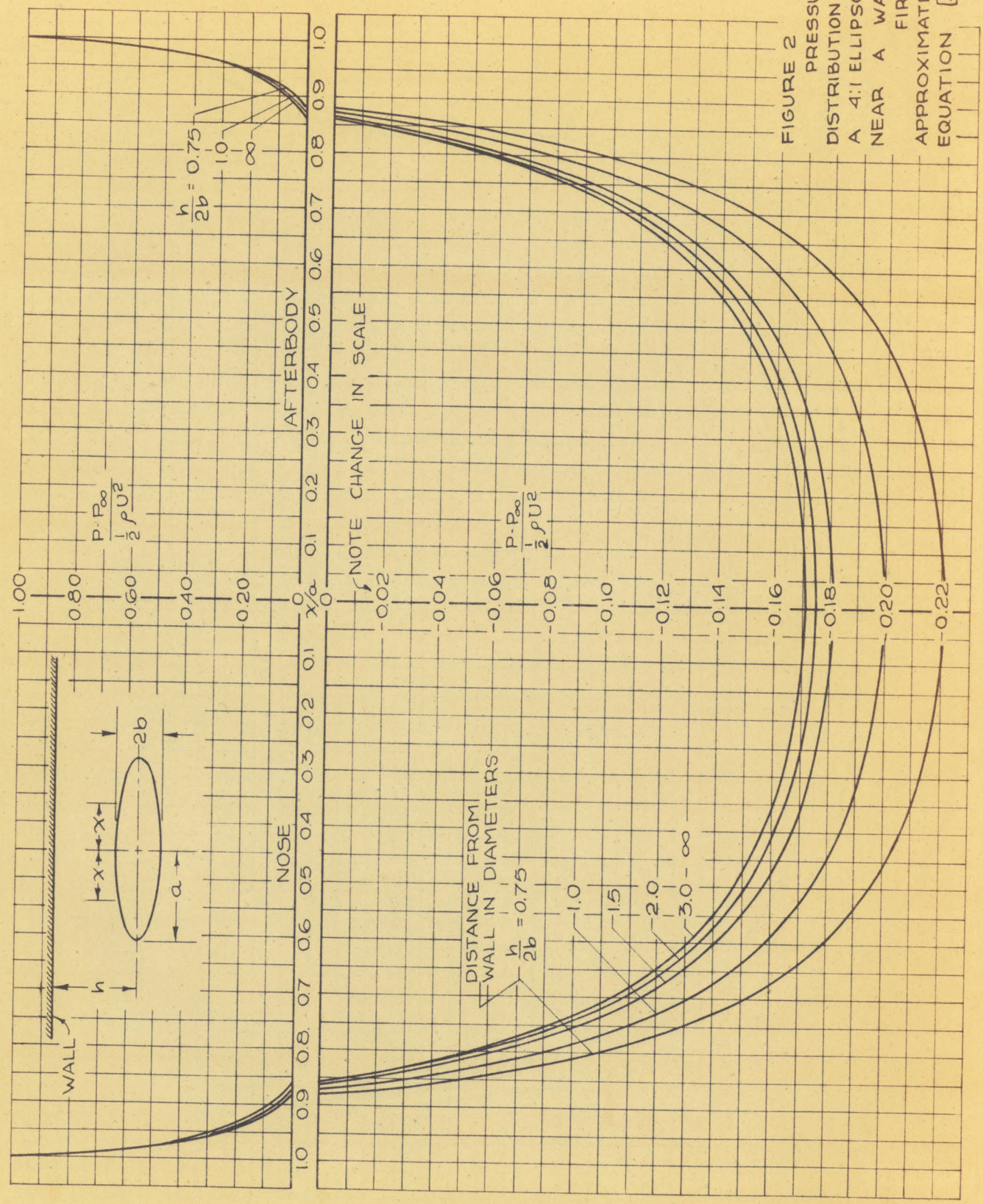

FIGURE 2
PRESSURE DISTRIBUTION ON A 4:1 ELLIPSOID NEAR A WALL - FIRST APPROXIMATION EQUATION [35]

FIGURE 2

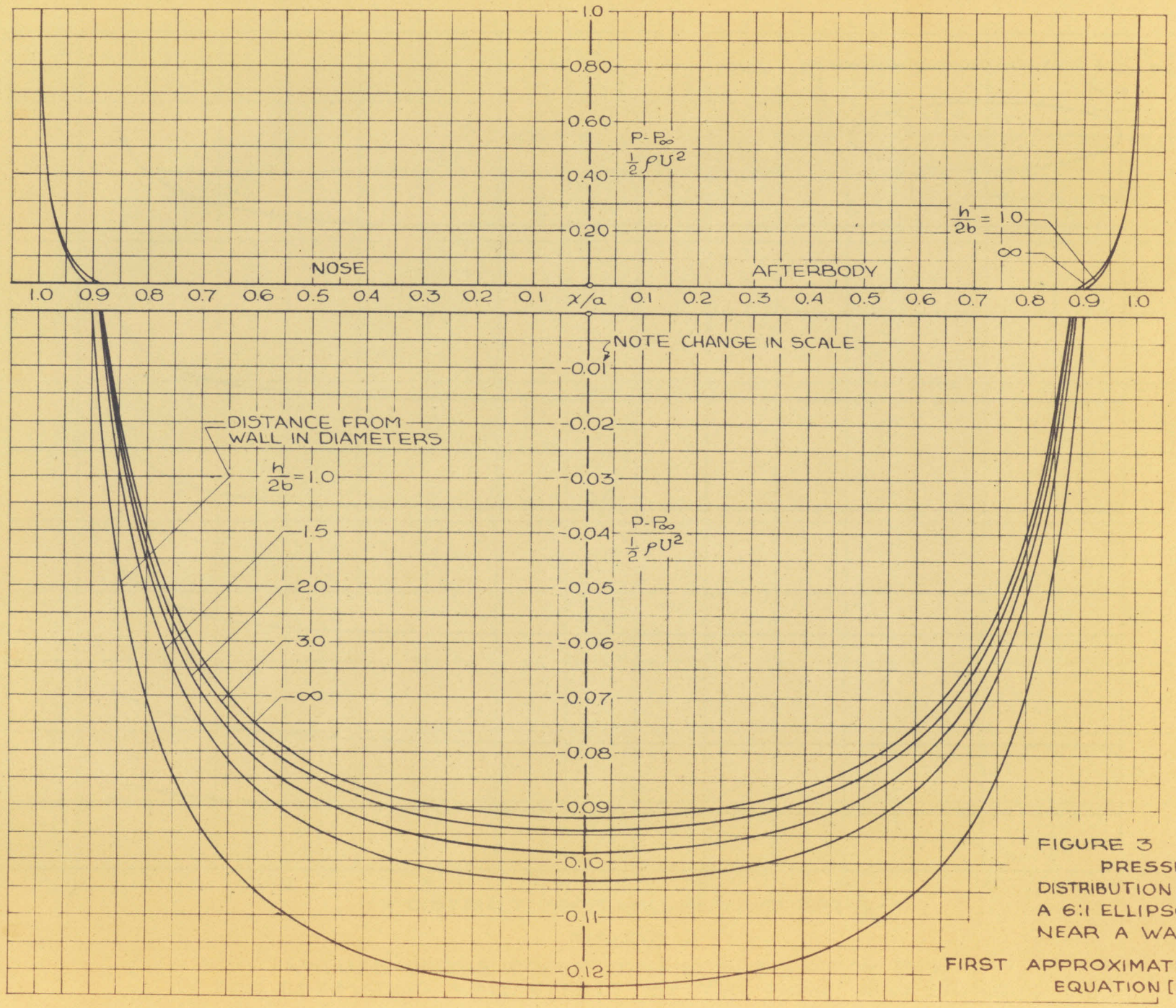

FIGURE 3
PRESSURE DISTRIBUTION ON A 6:1 ELLIPSOID NEAR A WALL-
FIRST APPROXIMATION, EQUATION [35]

FIGURE 3

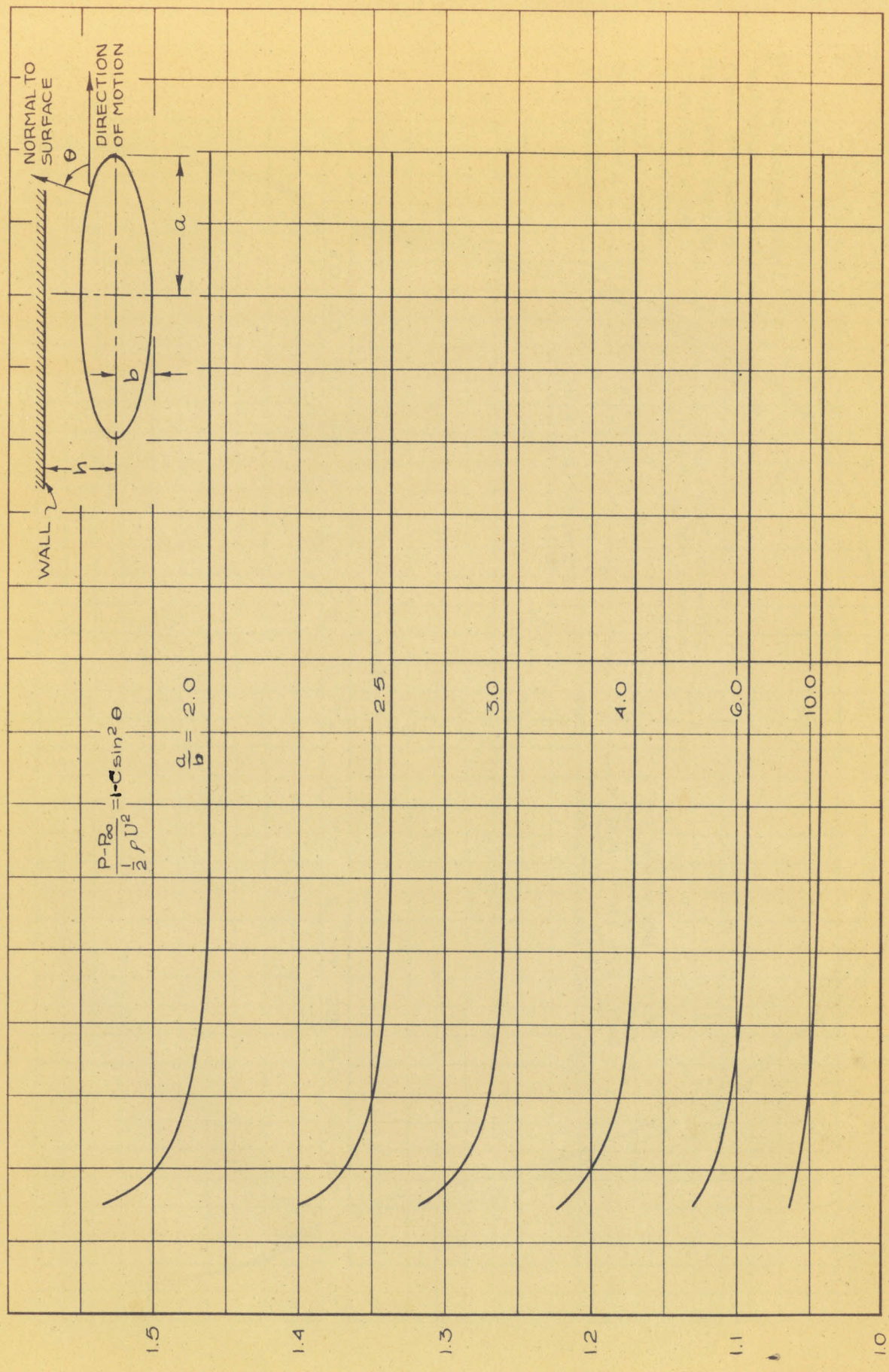

FIGURE 4

VALUES OF THE COEFFICIENT C IN EQUATION [35] - FOR ESTIMATING WALL EFFECT BY THE FIRST APPROXIMATION

FIGURE 4

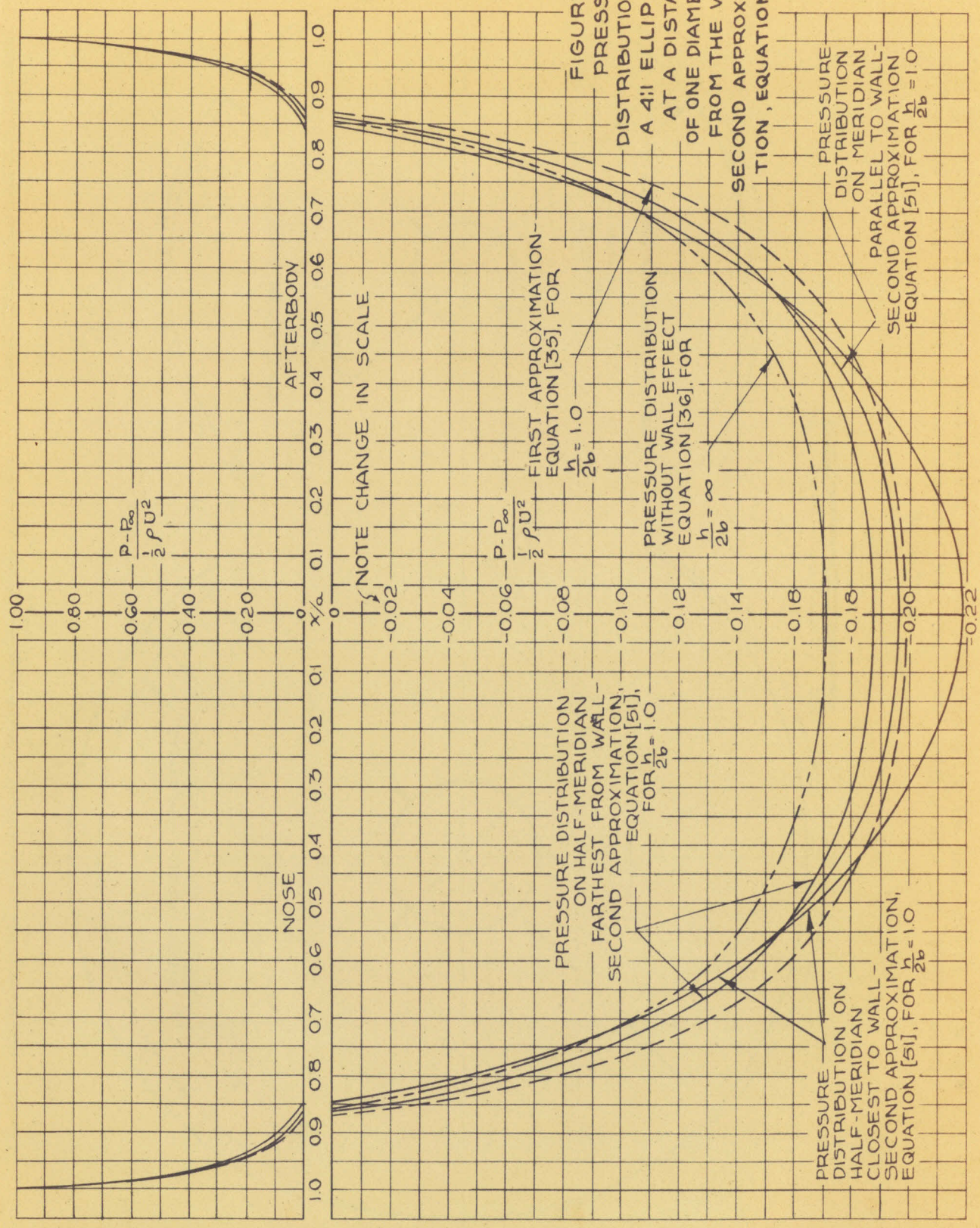

FIGURE 5 PRESSURE DISTRIBUTION ON A 4:1 ELLIPSOID AT A DISTANCE OF ONE DIAMETER FROM THE WALL SECOND APPROXIMATION, EQUATION [51]

FIGURE 5

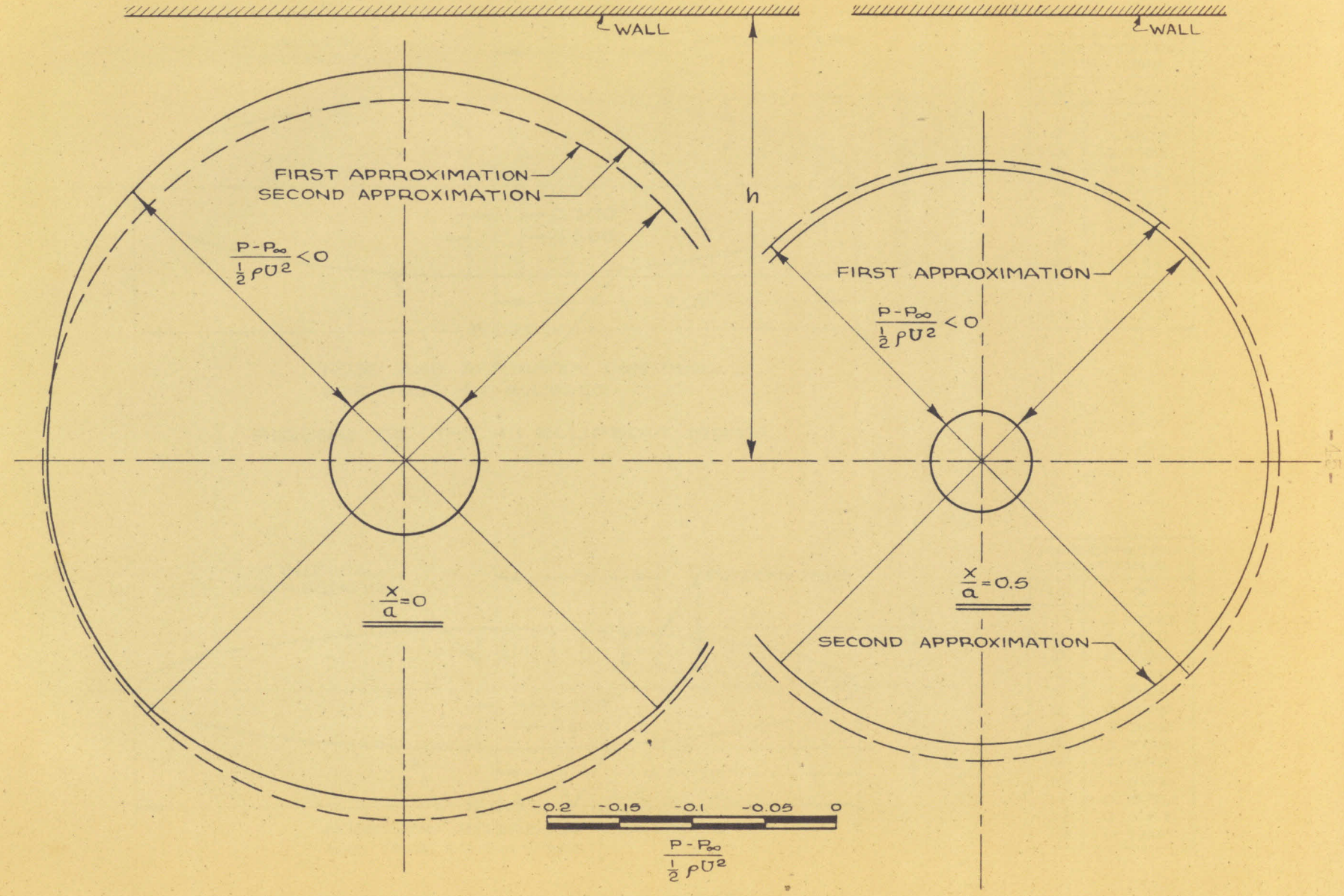

FIGURE 6

FIGURE 6
COMPARISON OF THE FIRST AND SECOND APPROXIMATIONS AT TWO STATIONS OF A 4:1 ELLIPSOID AT A DISTANCE OF ONE DIAMETER FROM THE WALL - $\frac{h}{2b} = 1$

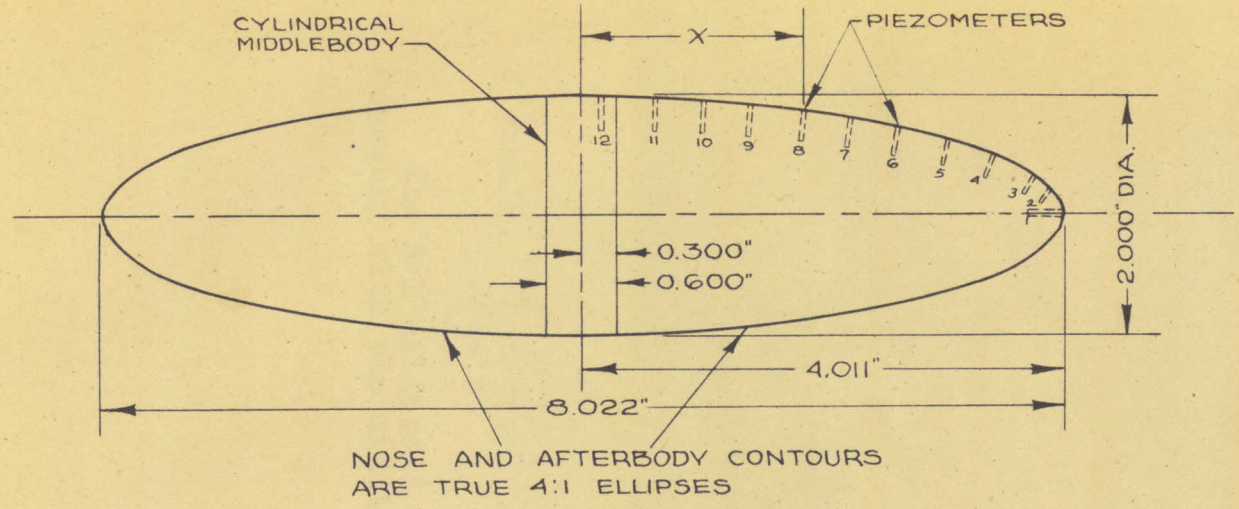

PIEZOMETER POSITIONS	
NO.	X"
1	4.011
2	3.903
3	3.740
4	3.413
5	3.048
6	2.645
7	2.242
8	1.840
9	1.441
10	1.038
11	0.638
12	0.156

FIGURE 7a THE 4:1 ELLIPSOID MODEL

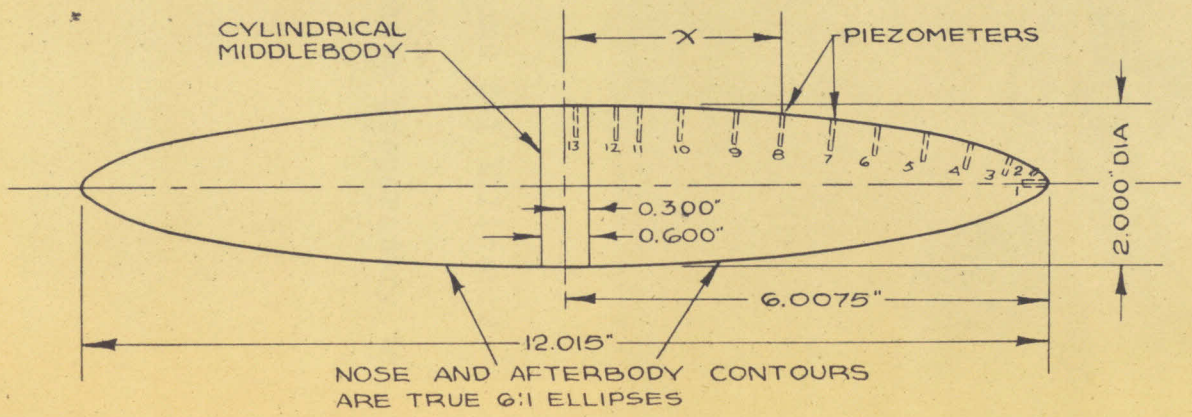

PIEZOMETER POSITIONS	
NO.	X"
1	6.0075
2	5.780
3	5.530
4	5.050
5	4.506
6	3.905
7	3.302
8	2.703
9	2.099
10	1.499
11	0.899
12	0.597
13	0.156

FIGURE 7b THE 6:1 ELLIPSOID MODEL

FIGURE 7 PRINCIPAL DIMENSIONS OF THE 4:1 AND 6:1 ELLIPSOID MODELS

FIGURE 7

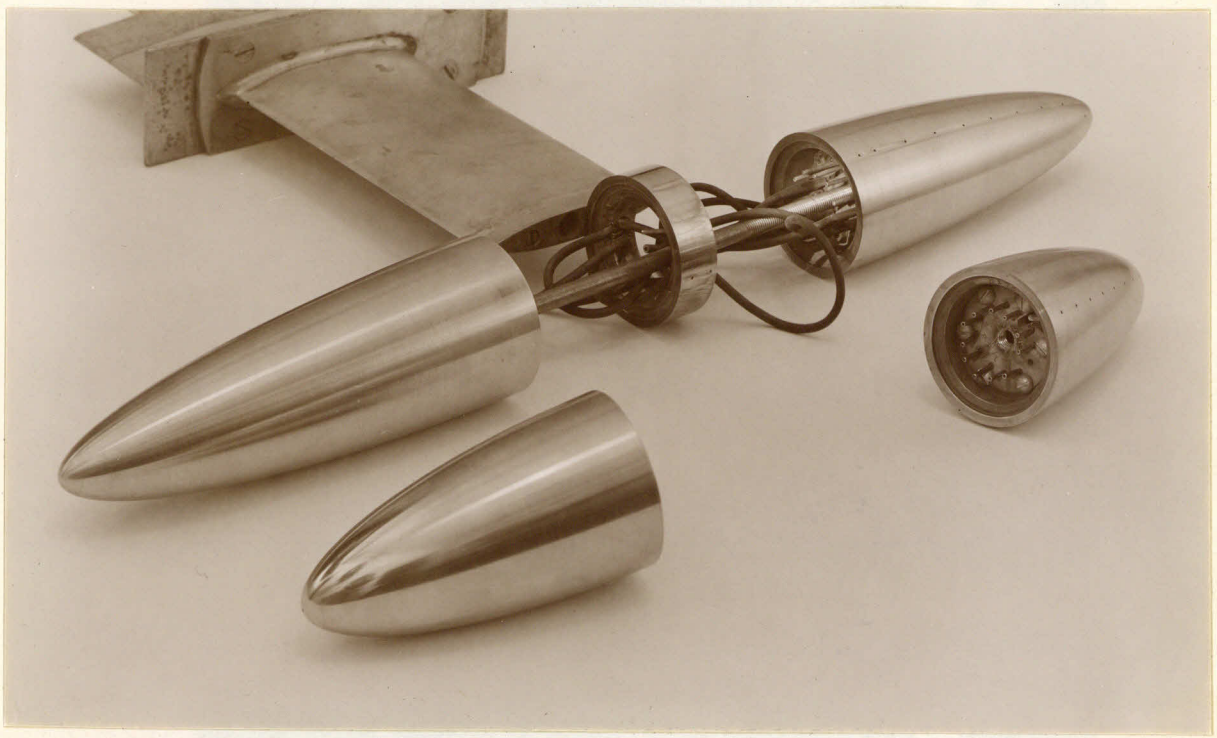

Figure 8. Photograph of the 4:1 and 6:1 Ellipsoid Models.

The 6:1 ellipsoid model is shown preparatory to assembly with the middlebody.

Figure 9. Photograph of the 4:1 Ellipsoid Model Mounted in the Free Surface Flume of the California Institute of Technology.

The model in this photograph is at a distance of one diameter from the plate. The water speed was 15.2 feet per second. Flow is from right to left.

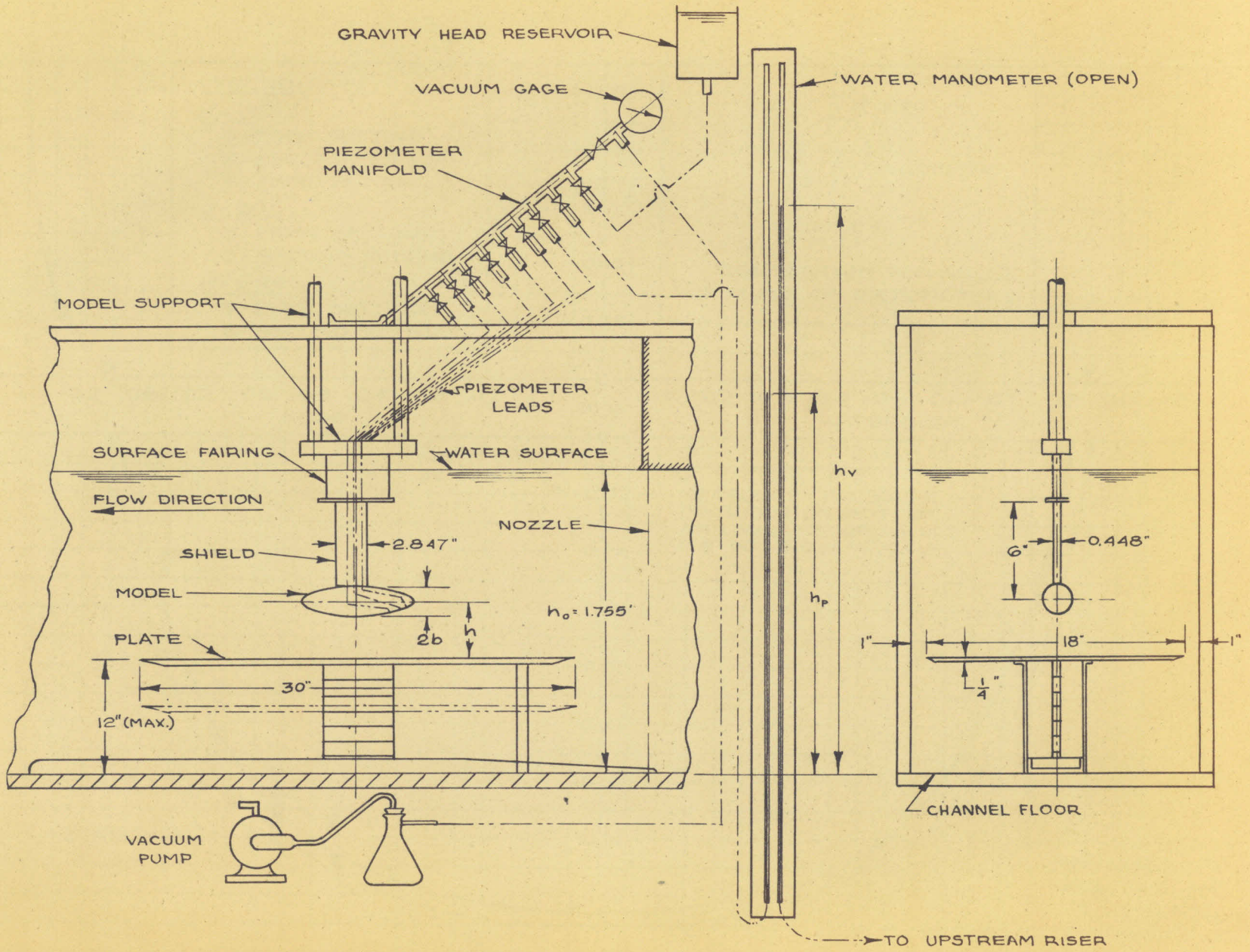

FIGURE 10

FIGURE 10 SCHEMATIC DIAGRAM OF ARRANGEMENT FOR PRESSURE DISTRIBUTION STUDIES IN THE FREE SURFACE FLUME

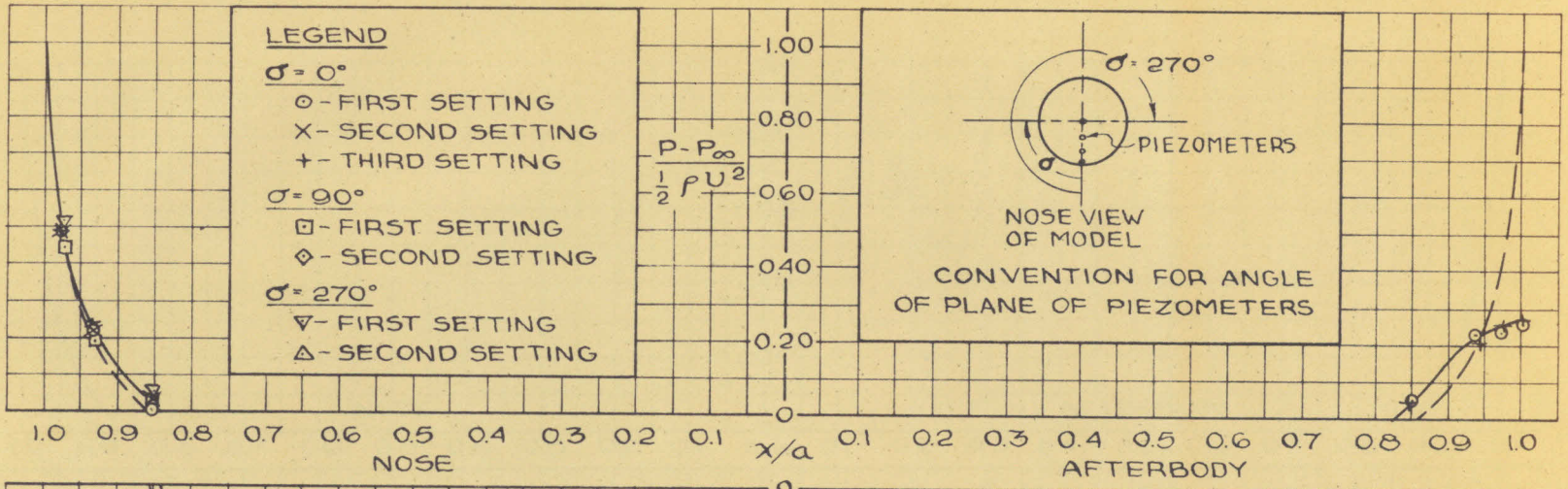

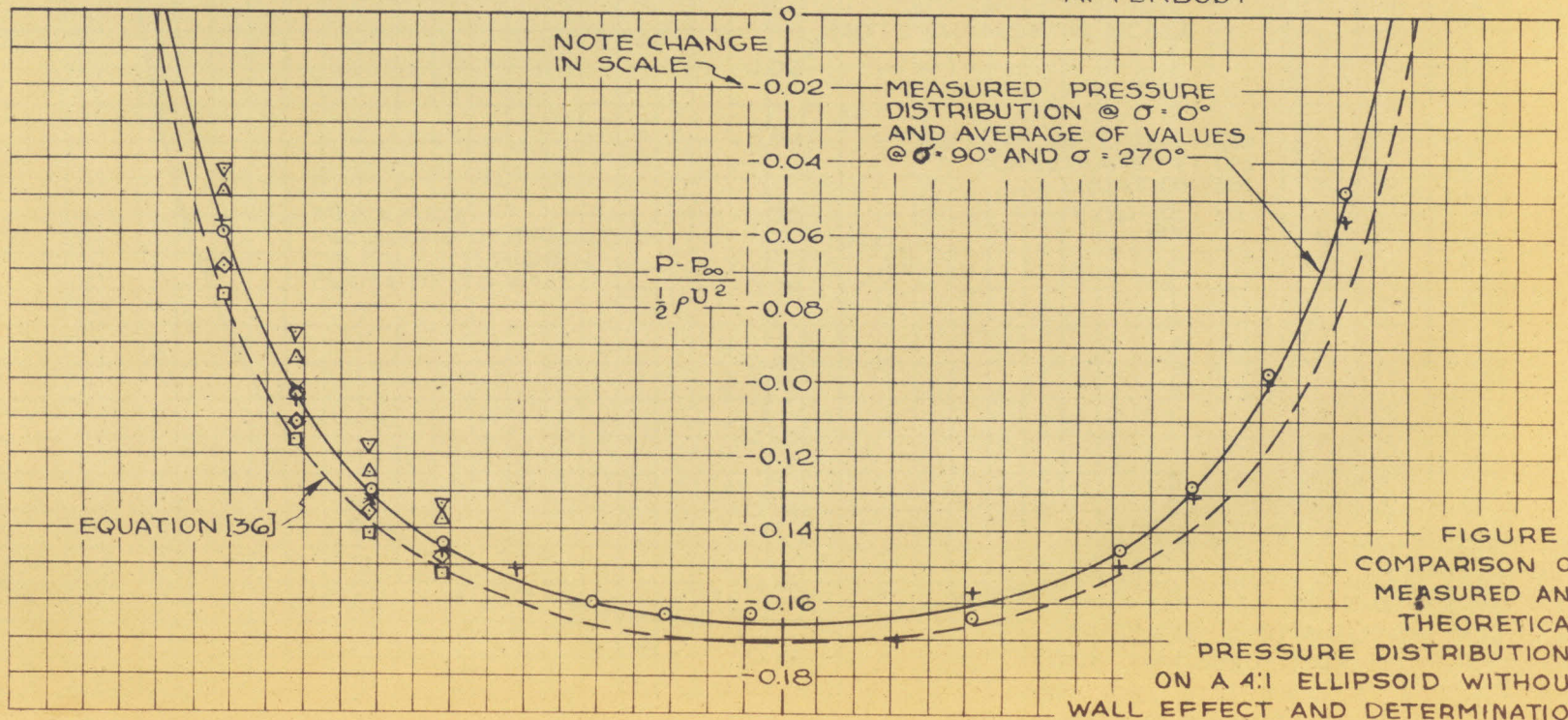

FIGURE 11

FIGURE 11
COMPARISON OF MEASURED AND THEORETICAL PRESSURE DISTRIBUTIONS ON A 4:1 ELLIPSOID WITHOUT WALL EFFECT AND DETERMINATION OF EFFECT OF SMALL YAW ANGLES

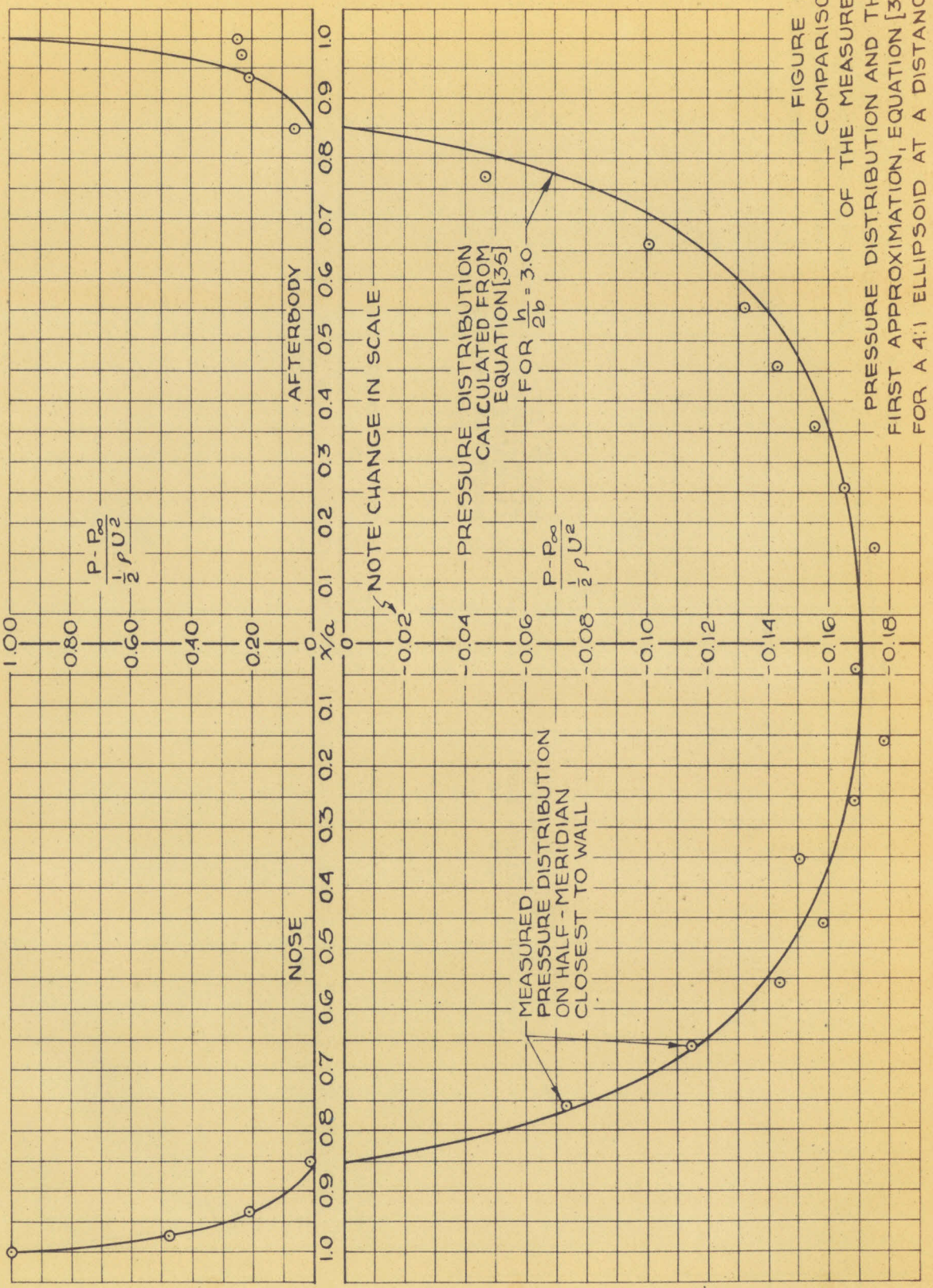

FIGURE 12
COMPARISON OF THE MEASURED PRESSURE DISTRIBUTION AND THE FIRST APPROXIMATION, EQUATION [35] FOR A 4:1 ELLIPSOID AT A DISTANCE OF 3.0 DIAMETERS FROM THE WALL

FIGURE 12

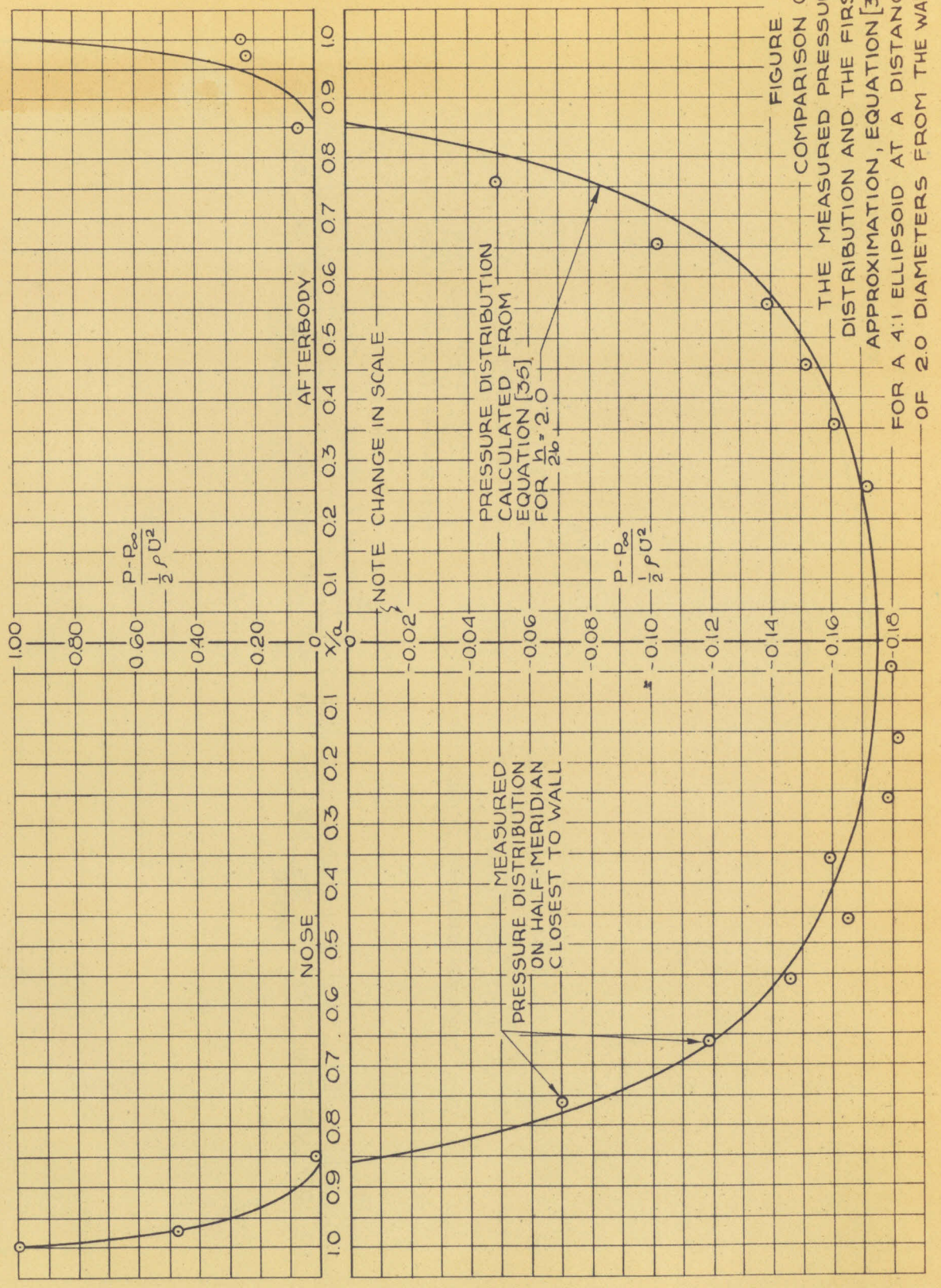

FIGURE 13
COMPARISON OF THE MEASURED PRESSURE DISTRIBUTION AND THE FIRST APPROXIMATION, EQUATION [35] FOR A 4:1 ELLIPSOID AT A DISTANCE OF 2.0 DIAMETERS FROM THE WALL

FIGURE 13

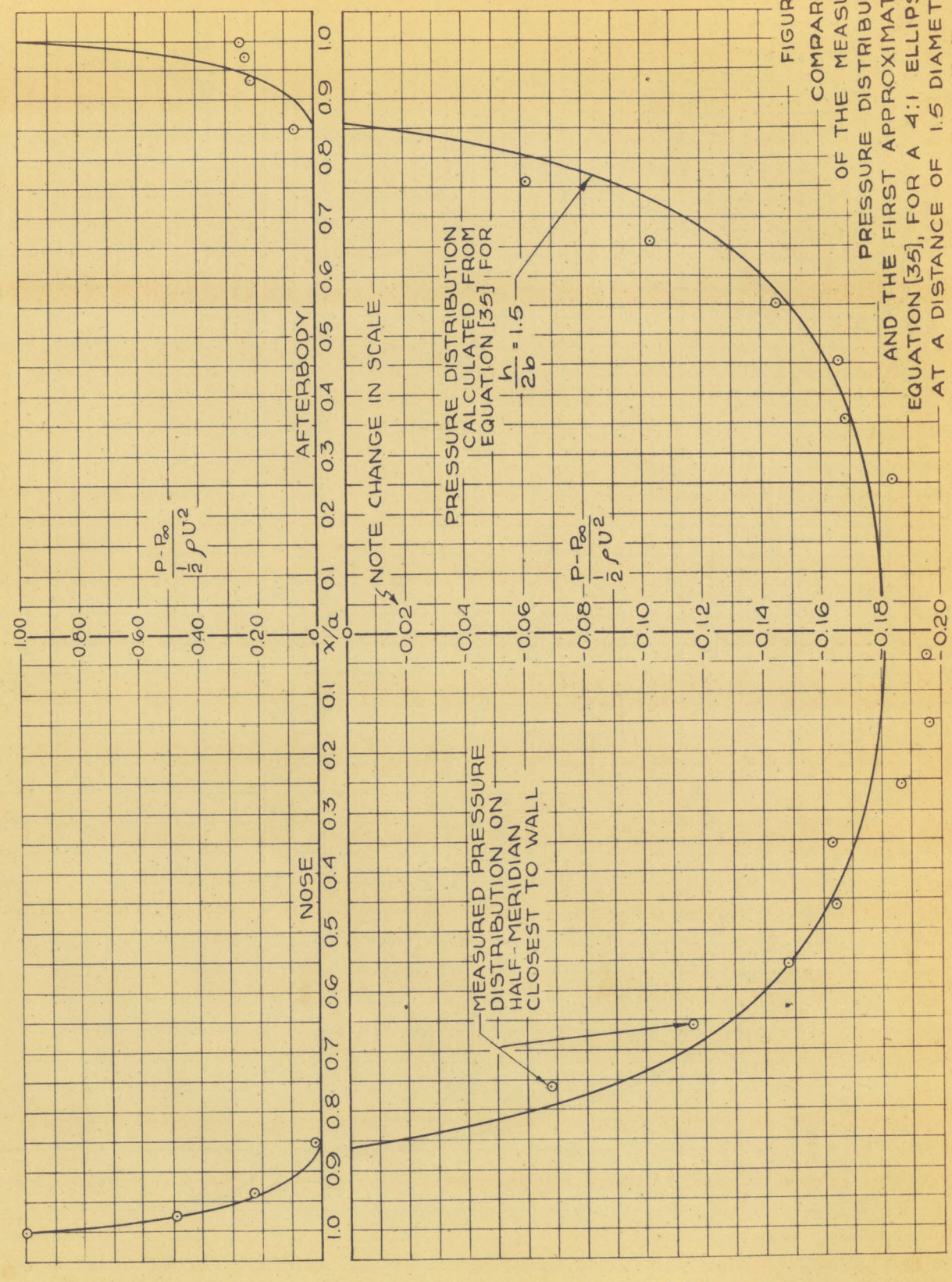

FIGURE 14 COMPARISON OF THE MEASURED PRESSURE DISTRIBUTION AND THE FIRST APPROXIMATION, EQUATION [35], FOR A 4:1 ELLIPSOID AT A DISTANCE OF 1.5 DIAMETERS FROM THE WALL

FIGURE 14

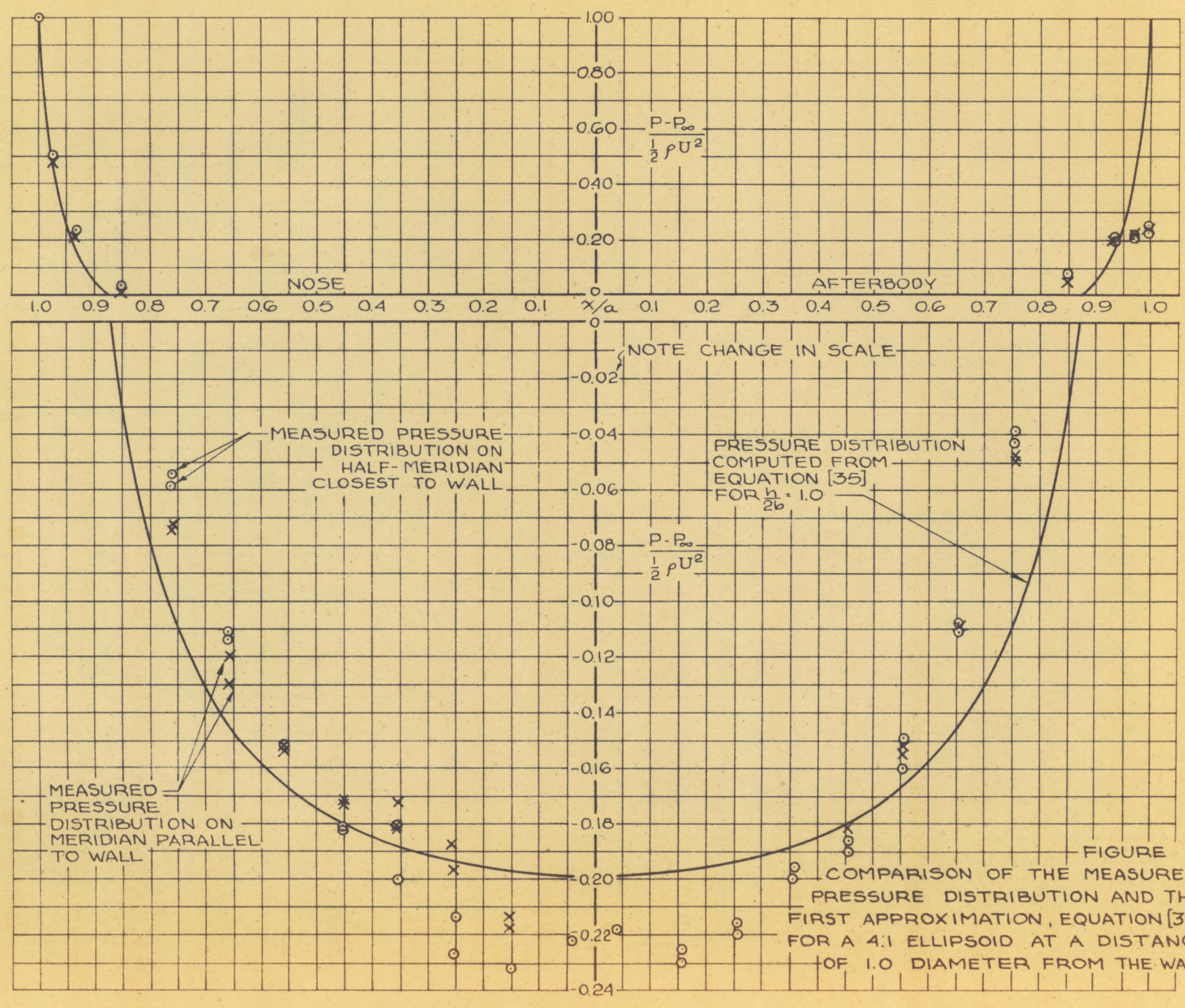

FIGURE 15

COMPARISON OF THE MEASURED PRESSURE DISTRIBUTION AND THE FIRST APPROXIMATION, EQUATION [35] FOR A 4:1 ELLIPSOID AT A DISTANCE OF 1.0 DIAMETER FROM THE WALL

FIGURE 15

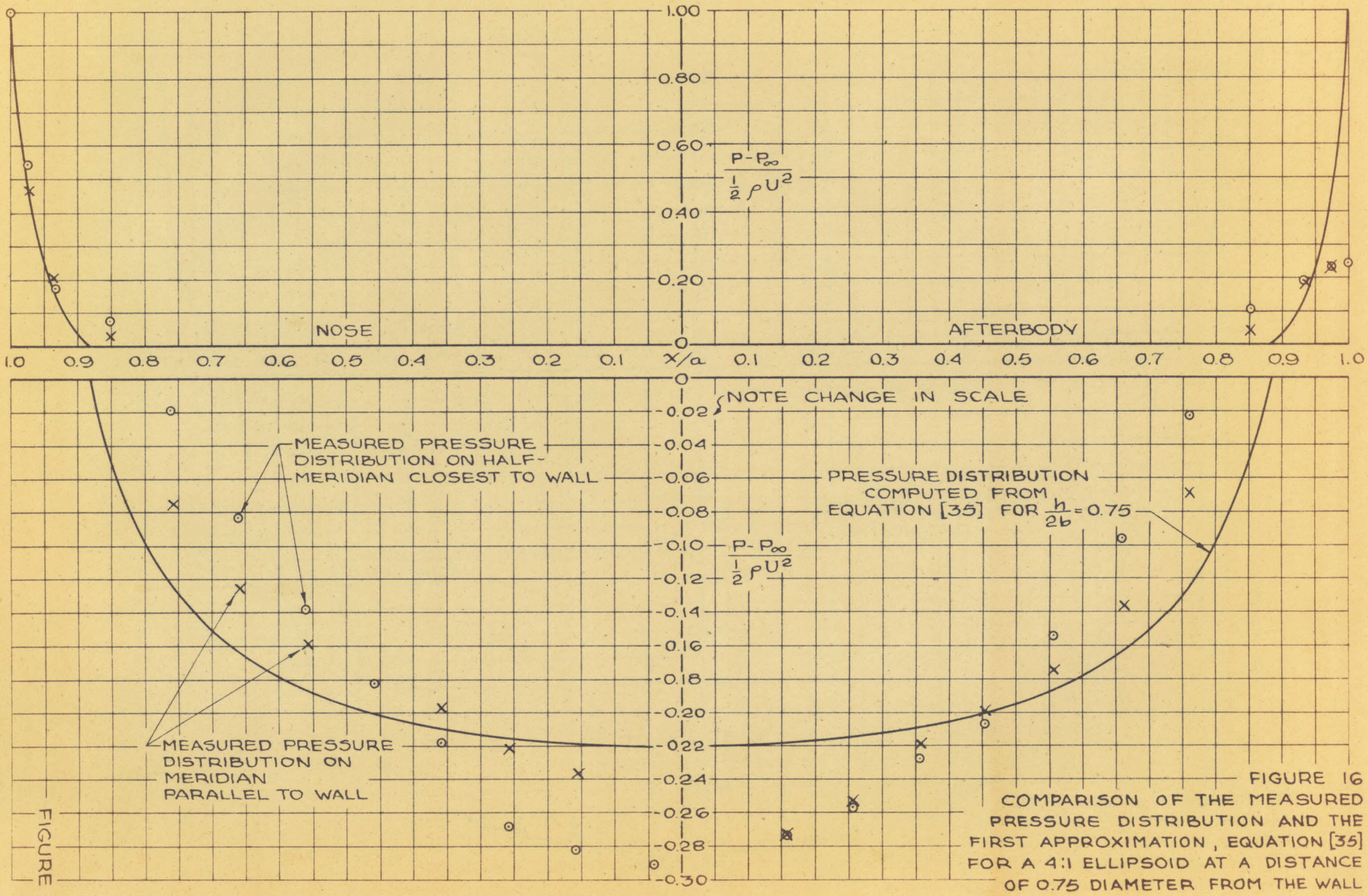

FIGURE 16

FIGURE 16
COMPARISON OF THE MEASURED PRESSURE DISTRIBUTION AND THE FIRST APPROXIMATION, EQUATION [35] FOR A 4:1 ELLIPSOID AT A DISTANCE OF 0.75 DIAMETER FROM THE WALL

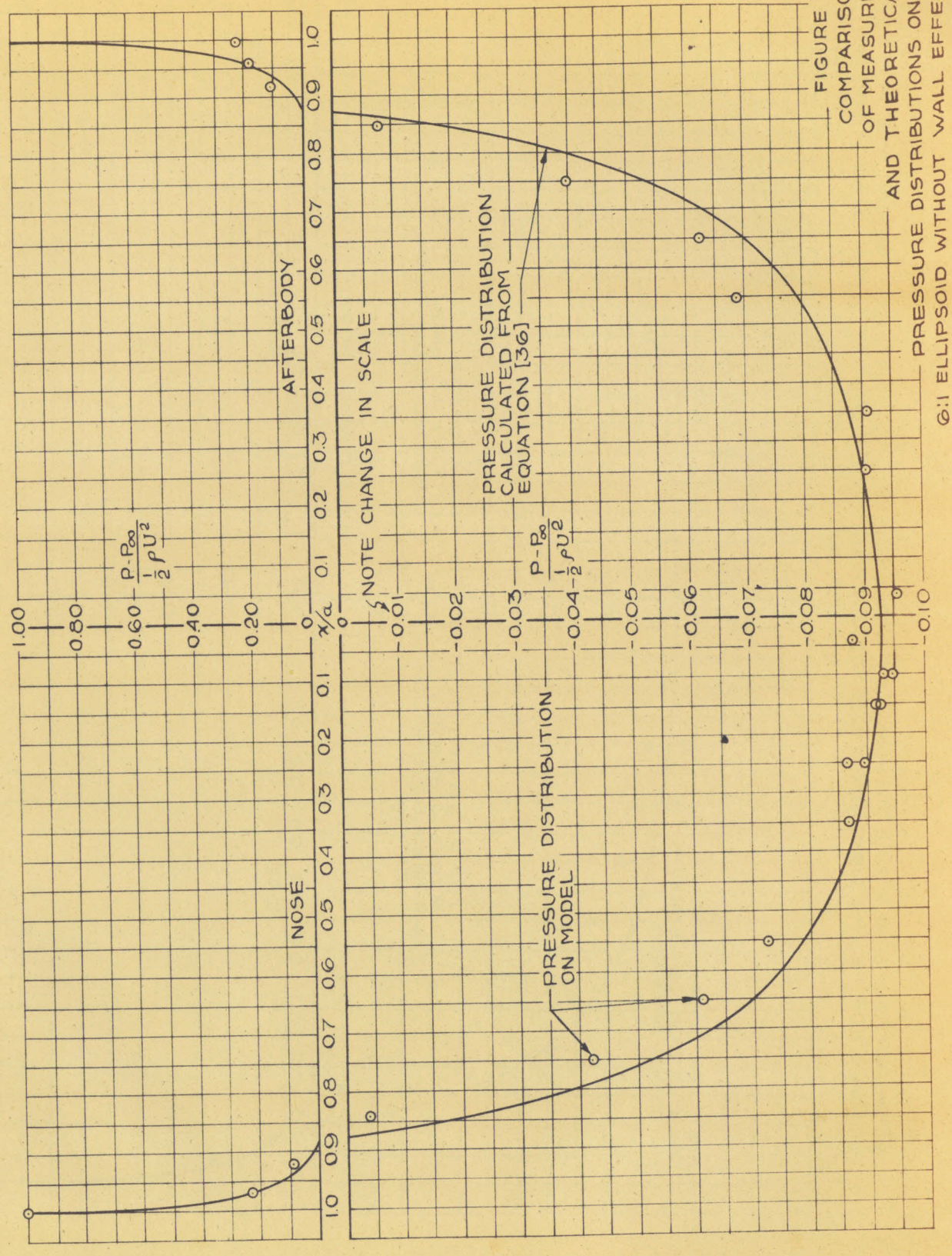

FIGURE 17
COMPARISON OF MEASURED AND THEORETICAL PRESSURE DISTRIBUTIONS ON A 6:1 ELLIPSOID WITHOUT WALL EFFECT

FIGURE 17

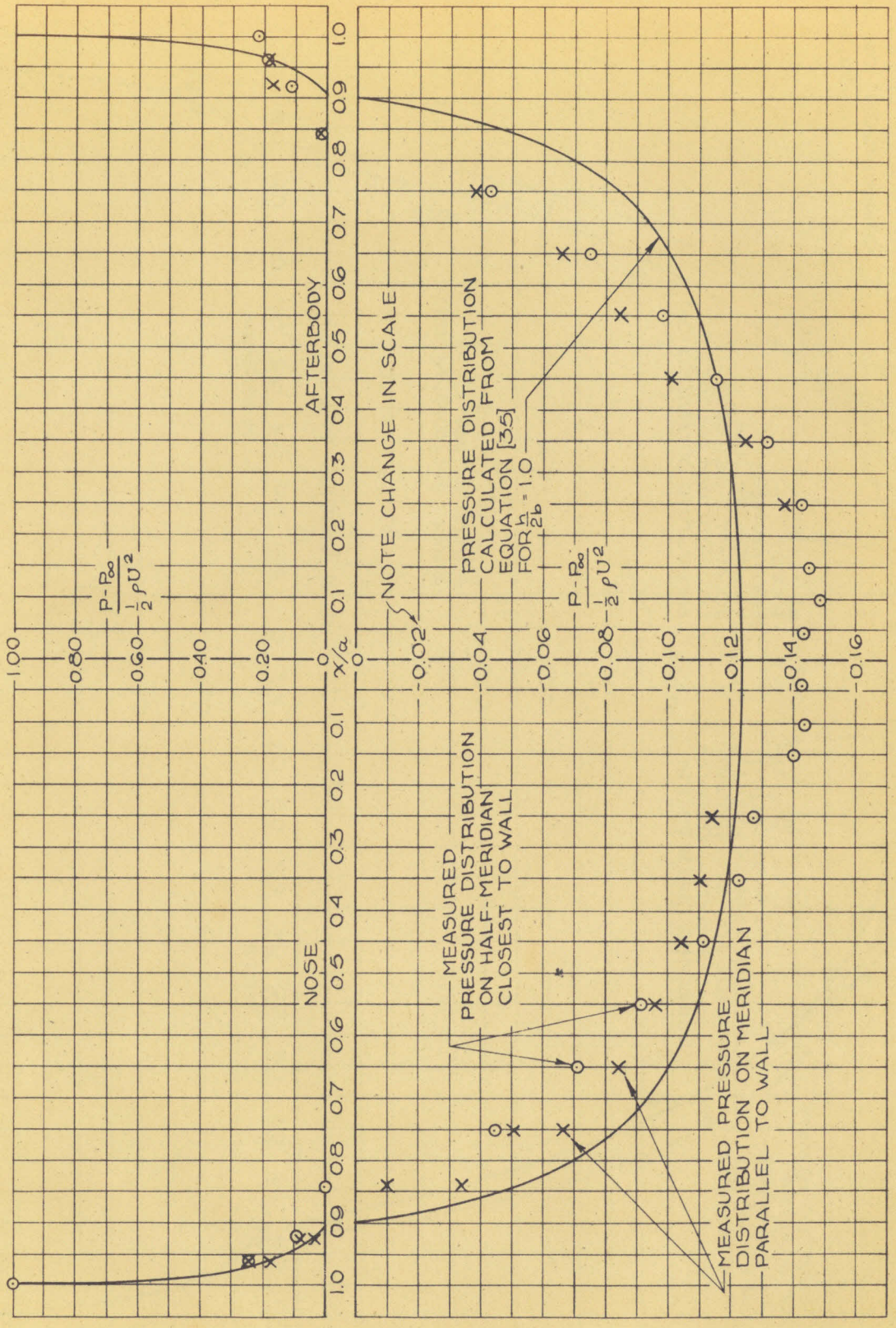

FIGURE 18

COMPARISON OF THE MEASURED PRESSURE DISTRIBUTION AND THE FIRST APPROXIMATION, EQUATION [35] FOR A 6:1 ELLIPSOID, AT A DISTANCE OF 1.0 DIAMETER FROM THE WALL

FIGURE 18

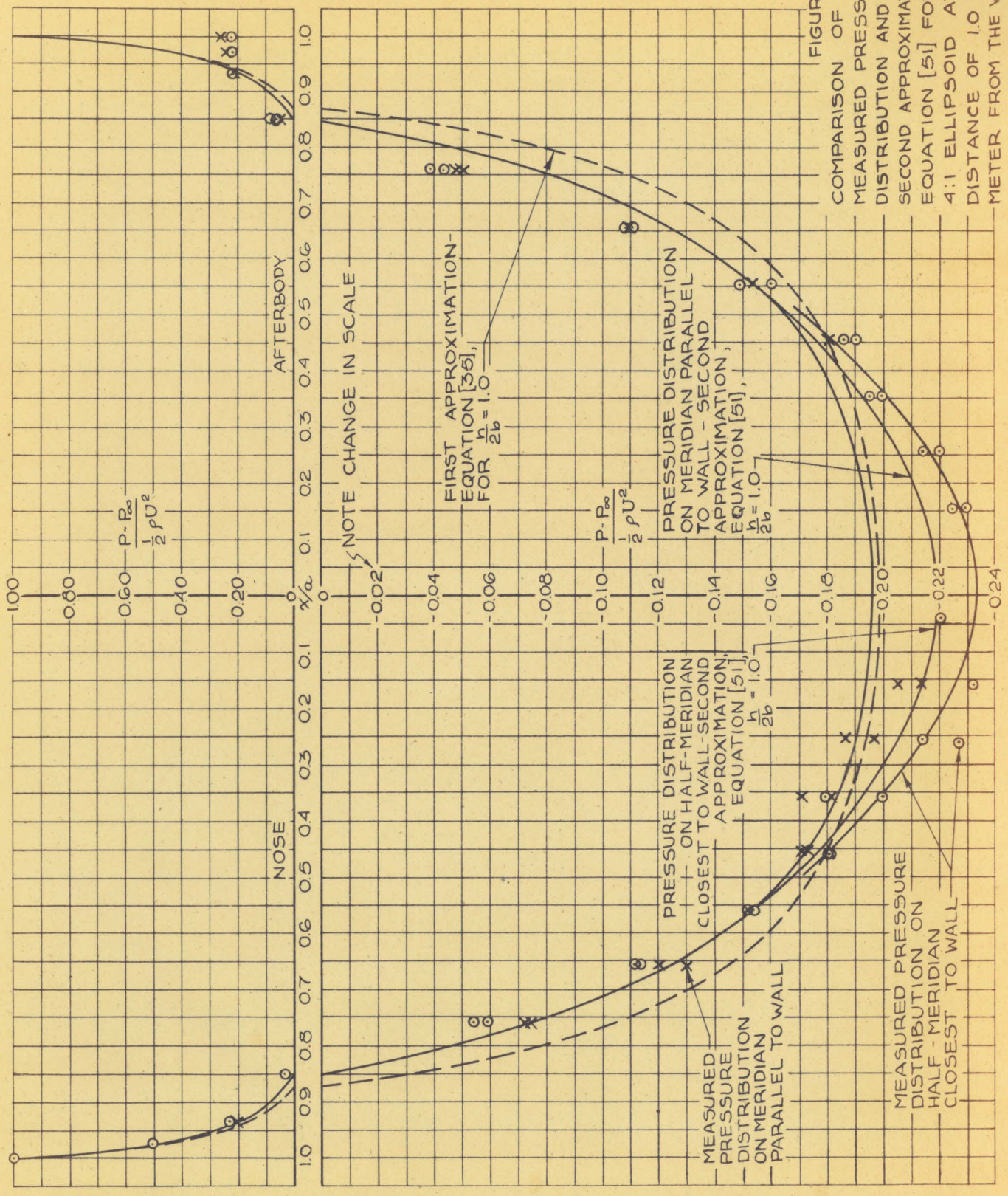

FIGURE 19
COMPARISON OF THE MEASURED PRESSURE DISTRIBUTION AND THE SECOND APPROXIMATION EQUATION [51] FOR A 4:1 ELLIPSOID AT A DISTANCE OF 1.0 DIAMETER FROM THE WALL

FIGURE 19